UNIVERSITY OF CALIFORNIA, SAN DIEGO

Multispectral Imaging and Analysis of a Transgenic Mouse Model of Pancreatic Cancer

A Thesis submitted in partial satisfaction of the requirements
for the degree Master of Science

in

Biology

by

Austin Robert Harrington

Committee in charge:

Professor Michael Bouvet, Chair
Professor James T. Kadonaga, Co-Chair
Professor Ella Tour

2017

The thesis of Austin Robert Harrington is approved, and it is acceptable in quality and form for publication on microfilm and electronically:

_____

_____

Co-Chair

_____

Chair

University of California, San Diego

2017

DEDICATION

This thesis has been a long time in the making; it is with deep gratitude with which I recognize the many people who have contributed to helping it come to fruition. I extend this gratitude to my family, who have unconditionally supported my educational goals; to my good friend and colleague Mai Khuong for being an inspiration and thoughtful judge of my work; to Professors Ella Tour and Lara Soowal for honing my skills as a scientist and instructor; to Jim Kadonaga for offering me my first job in a research lab; to Dr. Michael Bouvet for giving me the opportunity to perform research and continue my education; and particularly to Dr. Cynthia Snyder, my mentor, who trained me into the scientist I am today and whose standard of scientific and research excellence is the bar to which I compare both my own work and that of others.

EPIGRAPH

The most exciting phrase to hear in science, the one that heralds new discoveries, is not 'Eureka!' but 'That's funny...'

Attributed to Isaac Asimov

TABLE OF CONTENTS

Signature Page…….. iii
Dedication……..... iv
Epigraph……..... v
Table of Contents……..... vi
List of Abbreviations……. vii
List of Tables……..... viii
List of Figures……..... ix
Acknowledgements…….. x
Abstract of the Thesis…….. xi
Introduction……..... 1
Methods……..... 6
Results……..... 10
Tables……..... 18
Figures……..... 19
Discussion……..... 48
References……..... 59

LIST OF ABBREVIATIONS

C	PDX1-Cre transgene
CT	Computerized tomography
EGFP	Enhanced Green Fluorescent Protein
EMT	Epithelial-to-Mesenchymal Transition
FGS	Fluorescence Guided Surgery
GI	Gastrointestinal
H&E	Hematoxylin and Eosin
ICH	Immunohistochemistry
K	LSL-$Kras^{G12D/+}$ transgene (single knock-in)
LSL	Lox-Stop-Lox
mG	Membrane-targeted EGFP
MP	Multiphoton
MRI	Magnetic resonance imaging
mT	Membrane-targeted tdTomato
mTmG	Membrane-targeted tdTomato membrane-targeted EGFP transgene
P	LSL-$Trp53^{R172H/+}$ transgene (single knock-in)
PanIN	Pancreatic ductal intraepithelial neoplasia
PCR	Polymerase Chain Reaction
PDAC	Pancreatic ductal adenocarcinoma

LIST OF TABLES

Table 1. Spectral characteristics of selected fluorescent proteins……. 18

Table 2. Olympus OV100 illumination and filter specifications…….. 18

LIST OF FIGURES

Figure 1. Selected gross murine anatomy…… 19

Figure 2. Spectral characteristics and design of the PDX1-Cre/mTmG mouse model…… 20

Figure 3. Expression patterns of tdTomato and EGFP; gross anatomical imaging and findings of the PDX1-Cre/mTmG mouse model…… 21

Figure 4. Fluorescence microscopy of frozen and hematoxylin and eosin-stained paraffin-embedded sections of PDX1-Cre/mTmG pancreata detailing the pancreatic microenvironment…….. 26

Figure 5. Fluorescence microscopy of a paraformaldehyde-fixed whole pancreas and pancreatic microenvironment of the PDX1-Cre/mTmG mouse…… 27

Figure 6. Fluorescence microscopy of PDX1-Cre/mTmG mouse bowel sections detailing the small intestine and colon microenvironments…….. 28

Figure 7. Characteristics and design of the PDX1-Cre^{+}/Kras$^{G12D/+}$/ Trp53$^{R172H/+}$/ mTmG^{+} mouse model…… 32

Figure 8. Fluorescence imaging and histology of the CKPmTmG mouse model……. 33

Figure 9. Fluorescence microscopy of the CKmTmG whole pancreas and pancreatic microenvironment…… 38

Figure 10. Distribution of EGFP throughout the gastrointestinal tract by genotype……. 41

Figure 11. Histology and fluorescence microscopy of the CKmTmG large intestine microenvironment……. 44

AKNOWLEDGEMENTS

This thesis includes material currently published by: Cynthia S. Snyder, MD, Austin R. Harrington, BS, Sharmeela Kaushal, PhD, Evangeline Mose, BS, Andrew M. Lowy, MD, Robert M. Hoffman, PhD, and Michael Bouvet, MD, A Dual-Color Genetically Engineered Mouse Model for Multispectral Imaging of the Pancreatic Microenvironment. 2013; Pancreas.

ABSTRACT OF THE THESIS

Multispectral Imaging and Analysis of a Transgenic Mouse Model of Pancreatic Cancer

by

Austin Robert Harrington

Master of Science in Biology

University of California, San Diego, 2017

Professor Michael Bouvet, Chair
Professor James T. Kadonaga, Co-Chair

We intercrossed transgenic mouse lines to combine the mT/mG ("mTmG") dual-fluorescent reporter construct with the Cre variant PDX1-Cre ("C"). Successful inheritance of both transgenes resulted in offspring exhibiting bright and ubiquitous tdTomato expression in all tissues except in those with PDX1 activity (primarily pancreatic epithelium), which exhibited bright green EGFP fluorescence due to Cre-mediated excision of the tdTomato cassette. This new "PDX1-Cre/mTmG" line permits study of the pancreatic microenvironment and other tissues by color-coding epithelial and non-epithelial cell membranes therein, yielding exceptionally bright and crisp fluorescence images on both macroscopic and microscopic scales. PDX1-Cre/mTmG mice showed no apparent defects from these transgenes; the viability, overall health of the mice, and pancreata health and morphology were all typical of unmodified C57B/L6 mice. The PDX1-Cre/mTmG line was further developed to include the Cre-activated pancreatic

ductal adenocarcinoma (PDAC)-inducing transgenes LSL-Trp53^{R172H} ("P") and LSL-Kras^{G12D} ("K"). The new CKPmTmG mouse line produced color-coded, spontaneously generating pancreatic tumors. As with the PDX1-Cre/mTmG mouse model, the CKPmTmG mouse model enables bright and crisp fluorescence imaging. Final studies examined the effects of the activated Kras^{G12D} allele. All variants of the CKPmTmG model permit fluorescence imaging and study of the pancreatic microenvironment with unprecedented ease and image clarity.

INTRODUCTION

Cancer is a disease characterized by uncontrolled cell proliferation, invasion, and metastasis leading to morbidity and mortality. As of 2012 in the United States, cancer accounted for just under 23% of all deaths, second to only cardiovascular disease.[1] Pancreatic cancer is among the rarer forms of cancer; it represents only about 3% of cancer diagnoses each year and ranks as the 9th and 10th most common cancer for men and women, respectively. Despite its rarity, pancreatic cancer is among the most lethal types; it accounts for an outsized 7% of yearly deaths in the United States due to cancer (4th overall) and boasts a dismal five-year survival rate of approximately 6% post-diagnosis.[2] Several factors directly related to the disease itself contribute to these sobering statistics about the prognosis of pancreatic cancer, including its lack of early symptoms and typical late stage of diagnosis, aggressiveness of the malignancy, and location of the pancreas within the abdominal cavity. Chemotherapeutics and radiation therapy are only partially effective treatments; surgical resection of the primary tumor is usually not a viable treatment option, as nearly 80% of patients diagnosed with pancreatic cancer are ineligible for surgical resection of tumors due to widespread metastasis at the time of diagnosis. Prognosis and survival time are strongly correlated with both treatment aggressiveness and post-diagnosis treatment start-time delay;[3] additional complexities of the disease, including significant desmoplasia, relatively avascular internal structure, and the importance of the pancreas as a digestive organ, contribute to the inefficacy of medical treatment and increase risks associated with surgical treatment;[4] severe end-stage symptoms of pancreatic cancer leave most patients with no treatment options except palliative care.[5]

Among the most effective methods of combating any type of cancer are early detection and aggressive treatment; however, pancreatic cancer usually remains undetected until its end stages, at which time treatments are frequently rendered ineffective.

New risk assessments for pancreatic cancer screening are needed; currently, the only quantified factors known to increase the risk of an individual developing the disease are family history of pancreatic cancer, tobacco use, increasing weight and obesity, and previous diagnosis of pancreas-specific diseases including, but not limited to: type II diabetes, other glucose metabolism syndromes, and pancreatitis.[5] While these risk factors are easy to identify in patients, there are currently no specific screening criteria or methods specific to pancreatic cancer; imaging tests like computerized tomography (CT) and magnetic resonance imaging (MRI) could be used to examine at risk populations but carry additional externalities including high monetary costs and (for CT scans) potentially unnecessary radiation exposure. Though improvements in treatment have been made over the past decade, the rapid and devastating progression of pancreatic cancer coupled with limited early detection techniques and lack of curative treatments make a compelling case for new research into underlying disease mechanisms and targeted treatments.

Much about the development of pancreatic cancer is known, but to improve clinical outcomes of diagnosed pancreatic cancer cases, new insights into its biology are needed. Formally, the most common type of pancreatic cancer is referred to as pancreatic ductal adenocarcinoma (PDAC); like most cancers, PDAC develops over time as affected cells gain oncogenic mutations and lose tumor suppressor mechanisms. There are approximately four stages of abnormal cellular development within pancreatic acinar and surrounding ductal cells prior to classification as full-blown PDAC; these are classified (in order of increasing severity) as pancreatic intraepithelial neoplasia (PanINs) -1A, -1B, -2, and -3. Throughout the PanIN stages oncogenic mutations in K-ras, telomerase, and several others combined with loss of functions in p53, PTEN, and p16 tumor suppressors accumulate and change the function and morphology of a pancreatic lesion which may ultimately develop into fully malignant and metastatic dis-

ease.[5] After an initial PanIN-1 development, full-blown PDAC takes approximately seven additional years to develop if the process of mutation continues;[3] the early portion of this seven year window represents a critical period of potential detection which is often missed and for which new preventative screening methods are needed.

Unfortunately, as PDAC is typically detected at late stages of its development, large scale studies of early disease in humans are challenging to conduct due to the inherently small pool of available participants; thus, little is known about other physiological markers (and when to look for them) associated with the disease that may be used to aid in early clinical diagnoses. A partial solution to this problem is use of animal models of PDAC to examine the biology of the disease in a relatively close human relative; over the last ten years several advances have been made on this front, especially in mice. Two types of mouse models of pancreatic cancer are orthotopic injection models and orthotopic xenograft models; orthotopic injection models involve subcutaneous delivery of cancerous pancreatic cells suspended in cell culture medium into experimental mice, whereas orthotopic xenograft models involve surgical implantation of small pieces of pancreatic tumors into the pancreata of experimental mice. Medical and surgical treatments may be evaluated with these models of pancreatic cancer in addition to studying PDAC behavior and biology; tagging the injected cells or implanted tumor with an intravenously delivered fluorophore and combining fluorescence-guided surgery (FGS) with medical treatment has shown to be a promising proof-of-concept treatment program that could translate into the clinic.[6,7] However, despite the promising results using orthotopic models of PDAC, these models do not accurately reproduce the disease; patterns of invasion and metastasis, as well as tumor morphology observed via histology, only modestly match known characteristics of human PDAC.[5]

To better recapitulate the human disease, many laboratories studying PDAC have developed genetic mouse models; among the most successful of genetic models

are those utilizing Cre recombinase under the control of the pancreas-specific promoter PDX1 to conditionally activate an oncogenic allele of Kras (Lox-Stop-Lox [LSL]-$Kras^{G12D/+}$, referred to as "K") and mutant Trp53 (LSL-$Trp53^{R172H/+}$, referred to as "P") in pancreatic epithelium (mice with all three genes are designated "CKP") by selectively recombing these transgenes via the Cre recombinase variant PDX1-Cre (referred to as "C"). These two genetic mutations are among the most common genetic abnormalities associated with human PDAC; in mouse models the $Kras^{G12D}$ and $Trp53^{R172H}$ mutations produce a PDAC phenotype which presents with aggressive invasion of local tissues and widespread metastasis, more effectively recapitulating the human disease than any other type of mouse model to date; CKP mice typically succumb to disease within six months of birth.[8] One weakness of this model to note is that the disease develops throughout the entirety of pancreatic epithelium, whereas in human PDAC, cancer develops at a single locus and invades the surrounding tissue; despite this flaw, CKP mice remain one of the best genetic PDAC models available. The epithelial-to-mesenchymal transition (EMT) precipitating invasion and metastasis during PDAC development is of great concern clinically as these processes directly contribute to disease morbidity and mortality. Though precise mechanisms remain unknown, the CKP model has provided considerable insight into the chronology of events involved with invasion and metastasis of murine PDAC; introduction of a transgenic yellow fluorescent protein gene ($Rosa^{LSL-YFP}$) conditionally expressed in pancreatic epithelium revealed early pancreatic cell EMT and cell dissemination long prior to development of full PDAC.[9] It is currently unknown if the early pancreatic cell EMT and cell dissemination findings of Rhim and colleagues are also present in the human disease, and further insights into early PDAC behavior will be needed before potential development of new treatments and diagnostic techniques.

Transgenic fluorescent protein expression and tagging has become a corner-

stone of recent animal research, especially in mice.[10-14] Among the most useful tools for fluorescently labeling specific tissues is the transgenic mT/mG (mTmG) gene, which conditionally expresses Enhanced Green Fluorescent Protein (EGFP) after Cre-mediated excision of tdTomato encoding exons.[14] We intercrossed mice bearing mTmG and PDX1-Cre to generate a dual-fluorescent mouse line with ubiquitous membrane-targeted tdTomato expression and conditional membrane-targeted EGFP expression in pancreatic epithelium; we named this the PDX1-Cre/mTmG mouse line.[15] This model has proven highly effective in studying the pancreatic microenvironment by clearly de-lineating between pancreatic epithelial cell membranes from surrounding non-epithelial tissue membranes; pancreatic epithelium expresses EGFP while stromal components of the pancreas (as well as all other tissues) express tdTomato. After developing and fully characterizing the PDX1-Cre/mTmG mouse line, we chose to generate a new mouse model of pancreatic cancer which combined the labelling advantages of the PDX1-Cre/mTmG line with an existing model of murine pancreatic cancer. To this end we intercrossed mice and generated the LSL-Kras$^{G12D/+}$/LSL-Trp53$^{R172H/+}$/mTmG/PDX1-Cre (CKPmTmG) mouse model of PDAC; this model accurately reproduced the CKP disease phenotype in mice as described by Hingorani and colleagues, in addition to fluorescently labeling all epithelium and developing tumors of the pancreas with EGFP fluorescence, while labeling all pancreatic stroma and non-pancreatic tissue with tdTomato fluorescence.

METHODS

Mice

The membrane-targeted mTmG reporter construct (Table 1) and our dual-fluorescent pancreas-targeted PDX1-Cre/mTmG mouse line have been previously described and maintained on the C57BL/6 mouse strain (Figure 1).[15] We intercrossed mice heterozygous for PDX1-Cre and homozygous for mTmG with a knock-in line heterozygous for both LSL-Trp53$^{R172H/+}$ and LSL-Kras^{G12D} transgenes to produce quadruple transgenic mice with a single copy of the PDX1-Cre, mTmG, LSL-Trp53$^{R172H/+}$, and LSL-Kras$^{G12D/+}$ transgenes. Mice bearing the LSL-Trp53$^{R172H/+}$ and LSL-Kras$^{G12D/+}$ transgenes were provided as a gift from the lab of Dr. Andrew Lowy (Department of Surgery, UC San Diego). Approximately one in sixteen offspring were expected to inherit all four transgenes; subjects that did not inherit all three heterozygous transgenes from parent mice were used as controls or as experimental mice when appropriate (specified in the relevant figures). Multiplex polymerase chain reaction (PCR) genotyping for PDX1-Cre and mTmG was performed as previously described;[15] PCR genotyping for LSL-Trp53$^{R172H/+}$ and LSL-Kras$^{G12D/+}$ was performed with primer sets donated by the Lowy Lab (UC San Diego Moores Cancer Center). DNA for PCR was isolated from tail cuttings collected from mice 2.5-4 weeks of age. All mice were maintained in facilities and used for research purposes in compliance with protocols approved by the Institutional Animal Care and Use Committee at the University of California San Diego, an AAALAC accredited research institution.

Brightfield and Fluorescence Imaging

Olympus OV100 and CRI Maestro EX multispectral fluorescence and brightfield imaging of whole-mouse and whole-organ samples was performed as previously described (Table 2).[15] The spectral profiles of tissue autofluorescence (liver, bile, gastrointestinal tract, pancreas) and fluorophore emissions (tdTomato, EGFP) detected by our

Maestro imaging system were used to selectively subtract specific wavelengths for imaging analysis.

Confocal and Multiphoton Microscopy

Confocal imaging of PDX1-Cre / mTmG mice has been previously described.[15] Additional confocal and multiphoton microscopy was performed on CKP mice and relevant controls. Tissue samples were fixed in freshly made 3.2% buffered paraformaldehyde for approximately 12-16 hours then transferred to a solution of phosphate buffered saline. Whole or partial organ samples were mounted on either planar slides or slides with a sample reservoir, depending upon the size and topography of a specific tissue. Confocal imaging for these samples was performed with a Nikon AR1 confocal microscope (EGFP excitation: FITC, 488nm; tdTomato excitation: Texas red, 595nm). Multiphoton imaging was performed on a Nikon A1+ Multiphoton Confocal Microscope.

Histology

PDX1-Cre/mTmG and CKPmTmG tissue samples were fix a minimum of 24hrs in 10% formaldehyde and processed as previously described by the histology core at the UC San Diego Moores Cancer Center.[15]

Tissue preparation and dissection

Mice were sacrificed via CO2 asphyxiation immediately followed by cervical dislocation. Subjects' limbs were then secured to a dissection tray, the fur wiped with 70% ethanol, and exsanguinated via a cardiac blood draw or severing of a major artery. A transverse midline cut was made through the skin from the hindgut to the sternum. The peritoneum and skin were separated with scissors; the skin was secured to the dissection surface. The peritoneum was opened with a transverse midline cut and secured to the dissection surface. Secondary exsanguination via severing of a major vein or artery was performed if the initial cardiac puncture was insufficient. After this point dissections varied depending upon the tissue of interest. Special procedures and dissection meth-

ods are detailed below.

For studies of the small and large intestines, the gastrointestinal tract was severed at the esophagus and the remaining bowel extracted from surrounding organs and connective tissue. For macroscopic imaging the tissue was arranged in a serpentine pattern from esophagus to anus or opened via single cut down the entire length of the organ and split into a series of strips. The “Swiss Roll” technique[34] was used to examine the bowel in its entirety or select regions for histology and confocal imaging. Select portions of duodenum were prepared as previously specified and used for confocal and multiphoton imaging.

Gastrointestinal Tract analysis

Using OV100 images detecting tdTomato, bowels were measured for length from the pyloric sphincter to the anus and divided into 10 sections of equal length. Each section was then measured for area. The corresponding GFP-bandpass detection image of the bowel was overlaid with the length and/or area markers generated from a corresponding tdTomato image. EGFP area was then measured in each of the 10 regions and normalized.

Images

Channeling filtering and signal intensity measurements for Maestro Cubes were performed within the Maestro imaging system software before secondary analysis in both standard ImageJ and Fiji/ImageJ. Images collected with the Olympus OV100 and Olympus MVX, Nikon A1+ Multiphoton, and Nikon AR1 confocal microscopes were analyzed and processed with ImageJ (standard), Fiji/ImageJ, and PhotoScape (Mooii Tech). Vector graphics were generated in Microsoft Publisher 2016, Microsoft PowerPoint 2016, and Inkscape.

Statistics

Statistical analysis was performed with Microsoft Excel 2016 and MaxStat Lite.

We used ANOVAs with Bonferroni pairwise ranking post-hoc tests to analyze relevant data.

Acknowledgements

This chapter includes material currently published by: Cynthia S. Snyder, MD, Austin R. Harrington, BS, Sharmeela Kaushal, PhD, Evangeline Mose, BS, Andrew M. Lowy, MD, Robert M. Hoffman, PhD, and Michael Bouvet, MD, A Dual-Color Genetically Engineered Mouse Model for Multispectral Imaging of the Pancreatic Microenvironment. 2013; Pancreas.

RESULTS

A Dual Fluorescent Mouse Model of the Pancreas

Mice carrying the mT/mG transgene (mTmG) and the Cre variant PDX1-Cre were intercrossed and produced mice of three genotypes: non-fluorescent mTmG negative (+/+ or WT; PDX1-Cre may or may not have been inherited), single-fluorescent mTmG positive/PDX1-Cre negative mice (mTmG), and dual-fluorescent mTmG positive/PDX1-Cre positive mice (PDX1-Cre/mTmG). Non-fluorescent and single-fluorescent mice served as imaging controls; dual-fluorescent mice were the primary group of interest. The general mechanism of PDX1-Cre-mediated recombination of this model is diagramed in Figure 2B. Multiplex PCR was used to determine genotypes (Figure 2C). The transgenes of interest had no apparent adverse effects on the life expectancy, viability, genotype ratios, and overall health of the mice inheriting any combination of mTmG and PDX1-Cre. Imaging studies showed fluorescent phenotypes established during embryogenesis are maintained throughout the life of the mice (data not shown).

Initial whole-mouse imaging studies were performed with adult PDX1-Cre/mTmG, PDX1-Cre negative/mTmG, and non-fluorescent littermates of the same age using the Olympus OV100 (Table 2) and CRI Maestro EX imaging systems; this permitted uniformity of imaging exposure times and illumination intensity. Mice in the PDX1-Cre/mTmG line were expected to present with ubiquitous tdTomato expression except in tissues and cells with PDX1 activity, where Cre recombination to EGFP should occur. This tissue-specificity occurred as expected, with EGFP expression was limited to the pancreas, proximal duodenum, and antral stomach; co-excitation and of tdTomato and EGFP, a unique and useful feature of the PDX1-Cre/mTmG model, is also observed (Table 1, Figure 3A).

Fluorescence emission curves of EGFP, tdTomato, and autofluorescence of

relevant tissues (gastrointestinal wall, pancreas, liver) and fluids (bile) of this mouse model were collected via the Maestro EX imaging system (Figure 2A). Subtraction of autofluorescence spectra was achieved with the CRI Maestro EX imaging system (Figure 3B). Further examination of several tissues in PDX1-Cre/mTmG mice confirmed tdTomato expression across many different tissues not expected to have PDX1-Cre expression (Figure 3C) produced no EGFP. Extra-pancreatic PDX1-Cre activity was expected and observed (via EGFP expression) in the proximal duodenum and antral stomach (Figure 3D); PDX1-Cre activity gradually diminished down the length of the duodenum.

In PDX1-Cre/mTmG mice, PDX1-Cre recombination of mTmG from mT to mG in pancreatic epithelium was highly successful but not absolute. Cre recombination failure during pancreatic development resulted in tdTomato-expressing pancreatic epithelium in addition to the expected tdTomato-expressing stroma. This mosaic expression pattern was present in all PDX1-Cre/mTmG mice to at least a minor degree; rarely, mice exhibited highly mosaic pancreata with distinct regions of tdTomato-expressing epithelium visible at the macroscopic scale. A particularly extreme example of a mosaic pancreata is included in Figure 3E (Littermate 2); the pancreas of Littermate 1 in Figure 3E is representative of a typical PDX1-Cre/mTmG pancreas.

Initial confocal imaging of the PDX1-Cre/mTmG pancreas yielded impressive results; epithelial cell membranes were brightly labeled by EGFP and stromal membranes were brightly labeled by tdTomato (Figure 4A). Of the pancreatic epithelial cell types, acinar cells were most brightly labelled with EGFP; cell membranes within pancreatic islets were dimmer than those of acinar cells (dashed circle, Figure 4A), and individual duct cells and pancreatic ducts were difficult to distinguish from the extremely bright acinar cell fluorescence. Of the components of pancreatic stroma, vasculature scaffolding was the most prominent; a small vessel (red stripe, Figure 4A) and capillar-

ies interspersed throughout the tissue were clearly labelled by tdTomato. Fibroblasts, though stained with tdTomato, were more difficult to discriminate. Additional lower-magnification confocal imaging studies of the pancreas revealed Cre recombination failure occurs in discrete groups of cells within the tissue, indicating common lineage (Figure 4B). No cells exhibited both red and green fluorescence, which would result in a yellow fluorescence signal.

We performed additional confocal microscopy of the PDX1-Cre/mTmG pancreas with lightly-fixed whole tissue; this method of imaging permitted imaging of a significant portion of the whole pancreas surface area and smaller, highly magnified regions with approximately 30μm in depth (Figure 5). Pancreatic epithelium membranes were brightly stained with EGFP; acinar cells were easily identifiable; however, duct cells, pancreatic ducts, and islets were more difficult to discern with EGFP labelling alone (Figure 5, EGFP panel). Pancreatic stroma, particularly vascular scaffolding, was also effectively labelled by tdTomato per previous imaging; depth projection makes the overall organization of the vascular scaffolding readily apparent (Figure 5, tdTomato panel). As with previous imaging studies, pancreatic fibroblasts were difficult to discriminate.

Further imaging of additional tissues (proximal duodenum and proximal colon) of the PDX1-Cre/mTmG mouse model was our next step; as with the second phase of pancreas imaging, these tissues were lightly-fixed and directly imaged (Figure 6). Multiphoton imaging combined with the fluorescence of the PDX1-Cre/mTmG mouse model permitted nearly 200μm of depth penetration into the wall of the proximal duodenum and revealed much of the duodenal microenvironment (Figure 6A). Sporadic PDX1 activity in the duodenum was evidenced by the presence of both EGFP- and tdTomato-labeled epithelial cells membranes of the mucosal layer of the small intestine. Duodenal crypts extending to the submucosa are evident in the orthoslice and volume panels (Figure 6A). The outer muscularis externa and vasculature of the duodenum were

brightly labelled by tdTomato; both the longitudinal and circular smooth muscle layers of the small intestine were visible within the first 58μm of the tissue beneath the serosa (data not shown). Collagen was detected due to its generation of a second-harmonic signal (Figure 6A, Collagen panel). Spheroid clusters of EGFP-expressing epithelial cells indicated glands present within the submucosa (Figure 6A, Orthoslice and Volume panels), however, these could not be identified with certainty without additional markers from our data. Though relatively dark, cells adjacent to the EGFP-expressing epithelium expressed tdTomato; the reduced intensity is due to Texas Red laser calibration to the membrane-rich muscularis externa.

A cross section of the PDX1-Cre/mTmG small intestine showed a wide range of anatomical features; among the most prominent were villi, crypts, and muscularis externa (Figure 6B). PDX1 activity varies from villus to villus; some present with EGFP expressed throughout the entire epithelial layer while others appear to express tdTomato exclusively. The outermost layer of villi exhibited the expected columnar morphology and goblet cells of villi were indicated by their relatively large diameter and disbursal pattern. Lacteals and vasculature were present within villi and particularly apparent on the right side of the whole-lumen cross section.

The microenvironment of the PDX1-Cre/mTmG proximal large intestine was also examined (Figure 6C). The tissue appeared normal due to minimal PDX1-Cre activity, almost exclusively expressing tdTomato. Visible structures include the thick muscularis externa and thin internal muscularis mucosae; additionally, the mucosal folds and lamina propria of the proximal colon were present in the first three-quarters of a turn of the tissue in the outer layer of the sample. Additionally, EGFP-expressing clusters of villi were present; other than differing membrane fluorescence, these appeared identical to adjacent epithelium.

As fluorescent proteins may cause toxic effects within cells, we examined H&E

stained pancreata from PDX1-Cre/mTmG (dual-fluorescent, Figure 4C and 4D), mTmG (single fluorescent, data not shown), and C57BL/6 (non-fluorescent, data not shown) mouse lines. Histological findings of were normal in both the exocrine and endocrine regions of PDX1-Cre/mTmG and mTmG pancreata and comparable to those of non-fluorescent control mice (data not shown).

A Dual Fluorescent Mouse Model of Pancreatic Cancer

The next phase of the project began with the addition (via breeding) of two conditional knock-in genes, LSL-Kras$^{G12D/+}$ and LSL-Trp53$^{R172H/+}$, to the newly established PDX1-Cre/mTmG mouse model (Figure 7A); these mutations initiate and maintain pancreatic ductal adenocarcinoma in mice. Successful intercrosses resulted in mice carrying up to four transgenes: PDX1-Cre, mTmG, LSL-Kras$^{G12D/+}$, and LSL-Trp53$^{R172H/+}$; mice inheriting only one (CKmTmG or CPmTmG) or neither (CmTmG) of the PDAC-promoting knock-ins were assigned to control groups. In mice bearing both cancer-promoting knock-ins, morbidity appeared within the first several weeks of life; this proceeded to severe morbidity or mortality shortly thereafter (Figure 7B). CmTmG and CPmTmG control groups showed no outward signs of pancreatic disease within the first 24 weeks of life; over the course of many months (usually at least one year) the pancreata of CKmTmG mice consistently developed pancreatic dysmorphia and dysplasia characteristic of the PanIN stages of PDAC (Figure 8A, CKmTmG row; Figure 9).

Quadruple-transgenic, CKPmTmG mice developed dual-fluorescent pancreatic tumors which presented with a wide range of pathologic findings; these included pre-neoplastic and neoplastic changes characteristic of both the PanIN stages of PDAC development and the solid tumors and high-grade malignancy full PDAC (Figure 8). Initial findings indicated the dual-fluorescent tumors of CKPmTmG mice produced less intense EGFP fluorescence relative to the healthy pancreata of PDX1-Cre/mTmG mice. Three representative CKPmTmG mice (two males, one female) were selected for inclu-

sion; these mice were euthanized between 74 and 104 days of age. These mice were imaged via the Olympus OV100 in brightfield and fluorescence channels; pancreata were harvested and processed for H&E staining paraffin embedding.

The first CKPmTmG mouse included here was a male euthanized at 74 days of age with a large semi-solid dual-fluorescent fluorescent pancreatic tumor (Figure 8B). Fluorescence channels showed the tumor surface covered in highly-dilated duct-like structures (Figure 8B, iv, vii, ix, xi); the stromal scaffolding of these structures was apparent due to tdTomato fluorescence (Figure 8B, x). Histology of this tumor showed replacement of acini and encroachment upon islets by atypical ducts and desmoplasia (Figure 8, xii); also observed was widespread ductal atypia with focal luminal necrosis of ductal epithelium (Figure 8, xiii). The second CKPmTmG mouse of interest was a male euthanized at 104 days of age with a tumor composed of atrophied acinar tissue and serous cystic masses (Figure 8C, i-iii). Histological findings of this tumor were particularly wide-ranging and included multiple features of PanIN; neoplastic changes to pancreas morphology included papilliform (Figure 8C, iv), cribriform (Figure 8C, v), ductal atypia and duct-centered desmoplasia (Figure 8C, vi) leading to progressive isolation of islets (Figure 8C, vii). The final CKPmTmG mouse included was a female euthanized at 84 days of age with cystic and solid pancreatic masses (Figure 8D). Histological findings of this tumor included neoplastic changes associated with PanIN and high-grade malignancy closer to full PDAC; visible changes in semisolid regions of this tumor included atrophy and replacement of normal acini by proliferation and engorgement of atypical ducts in addition to desmoplasia (Figure 8D, iv, v). The solid region of this tumor showed many features of high-grade malignancy including nuclear atypia and a high mitotic rate (Figure 8D, vi).

Confocal imaging of the pancreatic microenvironment of a CKmTmG mouse euthanized at more than one year of age revealed striking features characteristic of the

PanIN-1A and PanIN-1B stages of PDAC development (Figure 9). The low-magnification whole-pancreas composite (Figure 9A) showed the effects of the $Kras^{G12D}$ allele on the pancreatic microenvironment in striking relief; pathologic features include enlargement of atypical ducts into cystic regions, dilated acinar and ductal clusters, and widespread desmoplasia. Islets appeared normal; other anatomical features included major vasculature, an intrapancreatic lymph node, and adjoining mesentery adipose.

Higher-magnification z-projections 40.5μm (Figure 9B, i-iii) and 39.0μm (Figure 9B, iv-vi) in depth demonstrated additional detail of the pathologic features of this pancreas. Much of the remaining epithelium attained a columnar phenotype, especially in cells bordering cysts and those in expanding duct structures; relative to normal pancreatic epithelium, acinar tissue was sparse in pancreata affected by $Kras^{G12D}$, indicating acinar atrophy and acinar-to-ductal metaplasia. Additionally, this pancreas exhibits significant desmoplasia and as such produced very bright tdTomato fluorescence; vascular proliferation and disorder was particularly evident. Fibroblast proliferation was difficult to discern due to its weak tdTomato fluorescence but nonetheless present. Higher magnification also enabled better examination of islets; though both epithelial and vasculature within islets was normal, they were isolated from surrounding tissue. Fluorescent mosaicism, a characteristic of the PDX1-Cre/mTmG mouse line, also occurred in the CKmTmG pancreas; of note were small regions of EGFP-expressing acinar tissue with normal morphology and small regions of tdTomato-expressing acinar tissue with normal morphology.

Mice which inherited the LSL-$Kras^{G12D/+}$ transgene presented with expanded EGFP expression in their gastrointestinal tracts. Rather than being confined to the proximal duodenum, EGFP was detected further down the length of the duodenum and occasionally in isolated patches throughout the ilium and jejunum; significant extra-

pancreatic EGFP expression occurred in the large bowel (Figure 10A). Analysis among the four genotypes of interest (CmTmG, CPmTmG, CKmTmG, and CKPmTmG) revealed statistically significant differences in EGFP expression were tied to the LSL-Kras$^{G12D/+}$ transgene (Figure 10B). These differences included overall EGFP expression and EGFP expression patterns throughout segments of the gastrointestinal tract (Figure 10B, iii-iv).

The large bowels of mice affected by the activated LSL-Kras$^{G12D/+}$ construct were examined for evidence of colorectal cancer; tissue was examined via confocal microscopy and histology (Figure 11). Confocal imaging revealed several anatomical features of the large bowel including the muscularis externa, muscularis mucosae, mucosal folds with columnar epithelium, lamina propria, and crypts; these structures primarily expressed tdTomato, though large regions of epithelium within the mucosa expressed EGFP (Figure 11A); no abnormal cell or tissue morphology was evident with fluorescence microscopy. Upon harvest one CKmTmG mouse was found to have a single polyp in the large intestine; the polyp was contained no EGFP-expressing cells and histological findings indicated it was non-malignant (data not shown). Examination via histology of large bowel walls from additional mice of the same genotype produced neither abnormal nor remarkable findings beyond large regions of EGFP expression (Figure 11B).

Acknowledgements

This chapter includes material currently published by: Cynthia S. Snyder, MD, Austin R. Harrington, BS, Sharmeela Kaushal, PhD, Evangeline Mose, BS, Andrew M. Lowy, MD, Robert M. Hoffman, PhD, and Michael Bouvet, MD, A Dual-Color Genetically Engineered Mouse Model for Multispectral Imaging of the Pancreatic Microenvironment. 2013; Pancreas.

TABLES

Table 1. **Spectral characteristics of selected fluorescent proteins**. Enhanced Green Fluorescent Protein (EGFP) and tdTomato; note that EGFP and tdTomato may be co-excited within a range of wavelengths on the blue-shifted flank of the tdTomato excitation curve.

Fluorophore Parameter	EGFP	tdTomato
Optimal Excitation Peak (nm)	488	554
Optimal Emission Peak (nm)	510	581
Excitation Efficiency at 488nm (%)	100	28
Excitation Efficiency at 554nm (%)	< 2	100

Table 2. **Olympus OV100 illumination and filter specifications**. The EGFP filter set permits excitation of EGFP and limited tdTomato excitation and detection of EGFP and tdTomato while the EGFP-Bandpass filter set blocks detection of tdTomato. The RFP filter set excites and detects in a range optimal for DsRed-derived proteins including tdTomato. EGFP-B, EGFP-Bandpass.

System Parameter	EGFP	EGFP-B	RFP
Excitation Range (nm)	460-490	460-490	535-555
Detection Range (nm)	≥510	510-550	570-625
Co-Excitation of tdTomato and EGFP	Yes	Yes	No
Co-Detection of tdTomato and EGFP	Yes	No	No

FIGURES

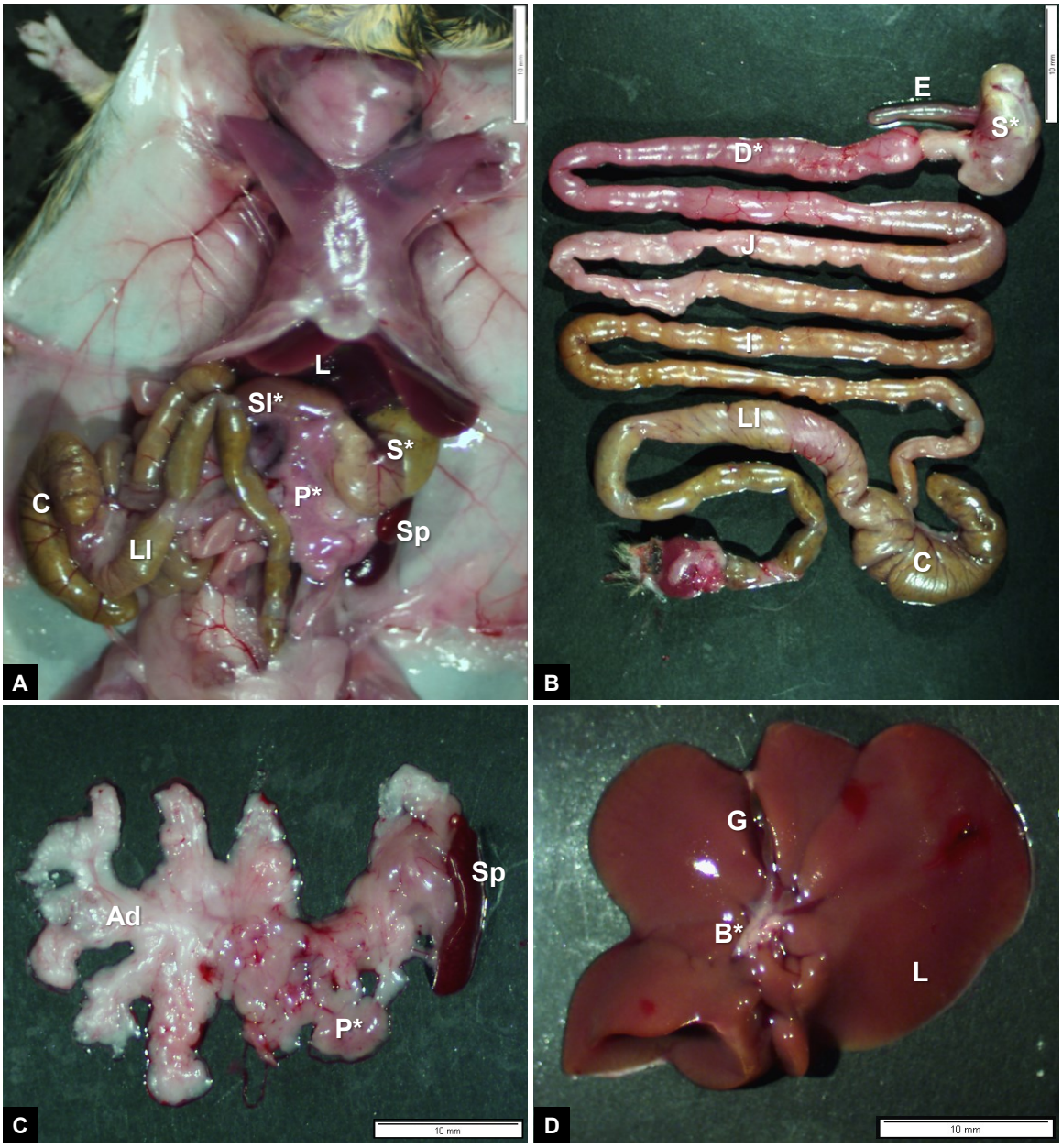

Figure 1. Selected gross murine anatomy. **A**, Abdominal cavity exposed in a healthy male control mouse. **B**, Partial gastrointestinal tract from (mid-esophagus to anus); anatomical divisions approximate. **C**, Pancreas detail; unlike the discrete human organ, the murine pancreas is far more diffuse and indistinct from adjoining mesentery and adipose tissue. The subtle hue change between the pancreas and mesenteric adipose indicates their boundary. **D**, Liver detail; the common bile duct runs through the pancreas and joins with the pancreatic duct forming the ampulla of Vater, through which bile, digestive enzymes, and ions drain into the duodenum. Asterisks (*) indicate areas of expected PDX1 activity during development; localization of PDX1 activity varies between and within specific tissue types. L, liver; SI, small intestine; P, pancreas; S, stomach; Sp, spleen; LI, large intestine; C, cecum; E, esophagus; D, duodenum; J, jejunum; I, ilium; Ad, mesenteric adipose; B, common bile duct; G, gallbladder.

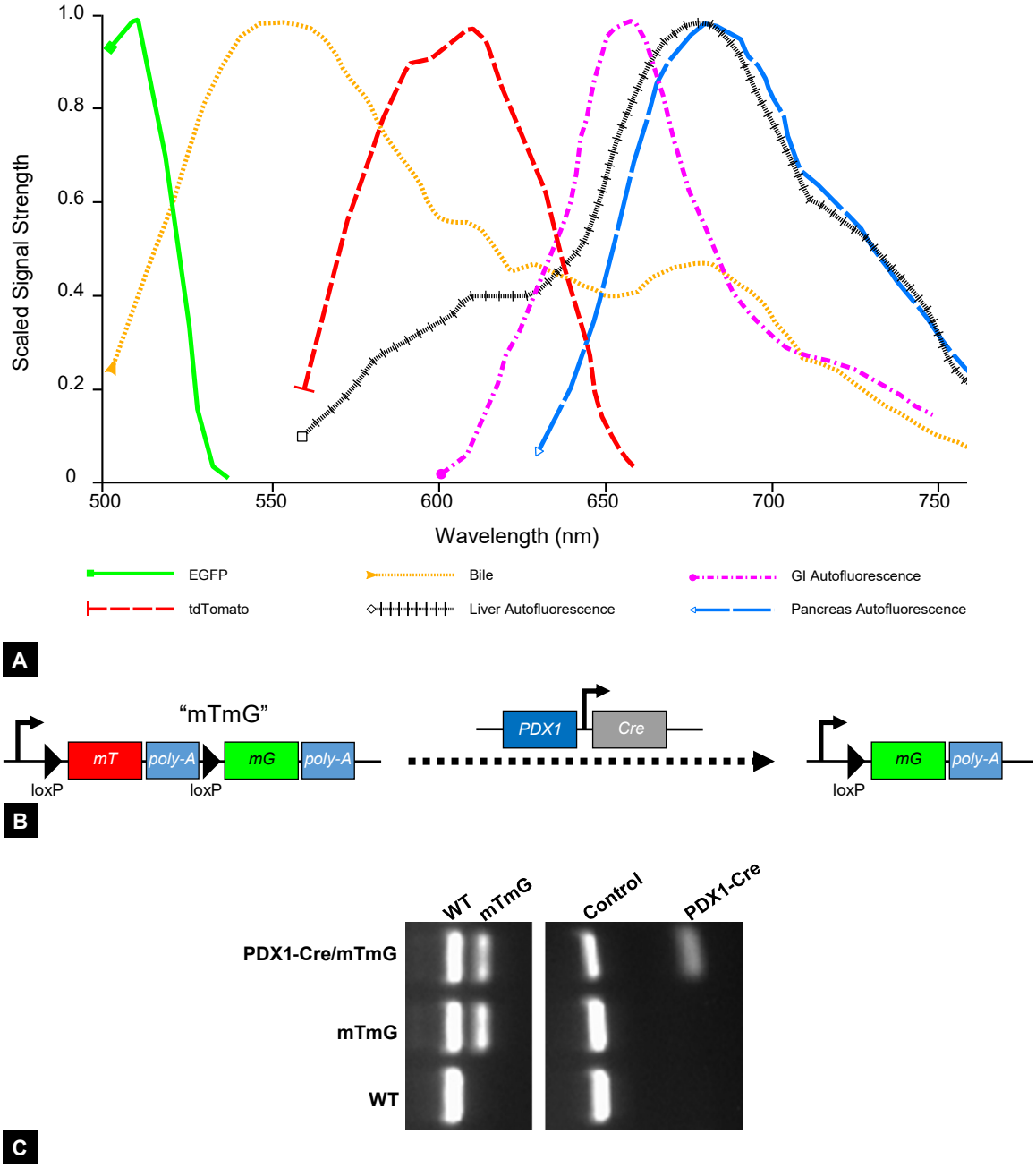

Figure 2. Spectral characteristics and design of the PDX1-Cre/mTmG mouse model. A, Fluorescent protein and autofluorescence emission spectra detected by the Maestro EX imaging system. Note the overlap of the EGFP and bile spectra; the Maestro excitation and emission process permits spectral separation of the overlapping EGFP and bile emission spectra unlike typical fluorescence imaging methods. Signals scaled to individual maxima. **B**, Diagram of PDX1 -Cre-mediated recombination of the membrane-targeted tdTomato and membrane-targeted EGFP ("mTmG") transgene, expressed under control of a CMV beta actin promoter at *ROSA26;* Cre expression in cells with PDX1 activity results in recombination of the mTmG resulting in the expression of EGFP. tdTomato is ubiquitously expressed in all other cells. **C**, Agarose gel of multiplex PCR genotyping of the PDX1-Cre/mTmG mouse model, control mice, and PCR controls.

Figure 3. Expression patterns of tdTomato and EGFP; gross anatomical imaging and findings of the PDX1-Cre/mTmG mouse model. Ubiquitous expression of tdTomato and tissue -specific expression of EGFP in wild type (WT) mice (bearing neither PDX1-Cre nor mTmG), mice carrying only mTmG, and mice inheriting both PDX1-Cre and mTmG. **A**, Olympus OV100 imaging under bright light (brightfield) and fluorescence channels (tdTomato and EGFP); arrows indicate pancreata. Mice were imaged at 6 weeks of age; livers and diaphragms removed. No fluorescence due to fluorescent proteins was detected in WT mice; gastrointestinal autofluorescence was detected in the EGFP channel. Mice with mTmG only displayed ubiquitous tdTomato expression in all tissues (including the pancreas); tdTomato is visible in the EGFP channel due to excitation overlap with EGFP and the OV100 filter. The final row of PDX1-Cre/ mTmG mice shows strong expression of EGFP throughout the pancreas and a mottled expression patterned in the proximal duodenum; all other tissues and pancreatic stroma (no PDX1 activity) exhibit tdTomato expression. **B**, Imaging obtained with the Cri Maestro EX imaging system of the same WT, mTmG, and PDX1-Cre/mTmG mice from **3A**. Composite images row shows total fluorescence emissions detected, (including autofluorescence). The second row shows the same images with autofluorescence spectra subtracted. **C**, Additional major organs harvested from a PDX1-Cre/mTmG mouse and imaged with the OV100 under brightfield (left) and fluorescence channels (tdTomato, right). tdTomato expression was found in all tissues; EGFP was not detected (data not shown) per the specificity of PDX1-Cre expression. Fluorescence imaging exposure time was identical in both channels. **D**, Extracted gastrointestinal tract (mid-esophagus to anus) of an adult male PDX1-Cre/mTmG mouse imaged with the OV100 under brightfield and fluorescence channels (tdTomato, EGFP, and EGFP bandpass). Adjoining organs including the pancreas, mesentery, kidneys, and reproductive organs were dissected away. EGFP is most prevalent in the superior duodenum in a mottled pattern; expression of EGFP gradually reduces moving down the small intestine. **E**, Pancreata of two PDX1-Cre/mTmG littermates. Littermate 1 presents with typical EGFP and tdTomato expression for PDX1-Cre/mTmG mice; littermate 2 presents with unusually high mosaicism of tdTomato and EGFP in the pancreas, indicating PDX1-Cre failure. P, pancreas; B, bowel; L, liver; St, stomach; Sp, spleen.

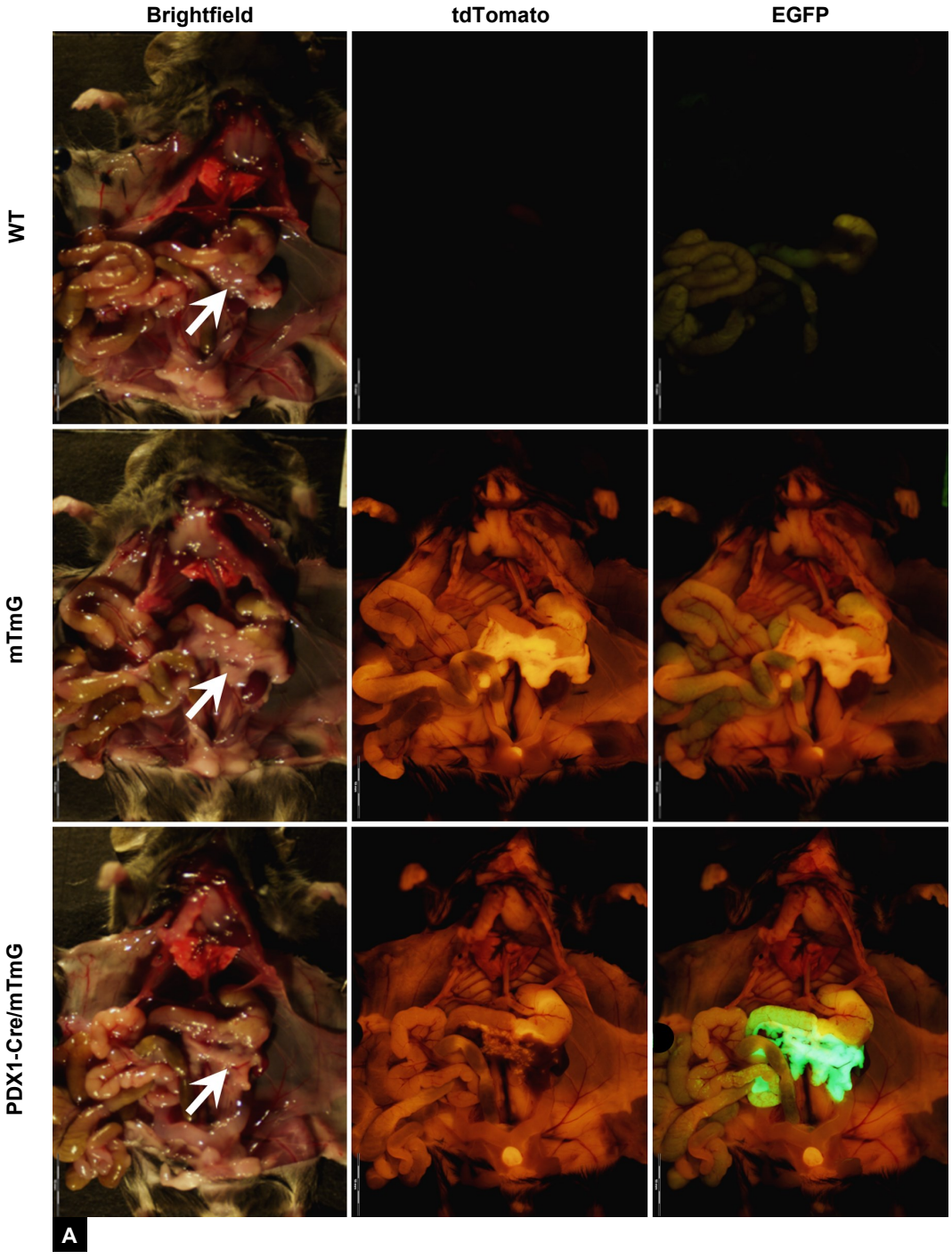
Brightfield
tdTomato
EGFP
WT
mTmG
PDX1-Cre/mTmG
A

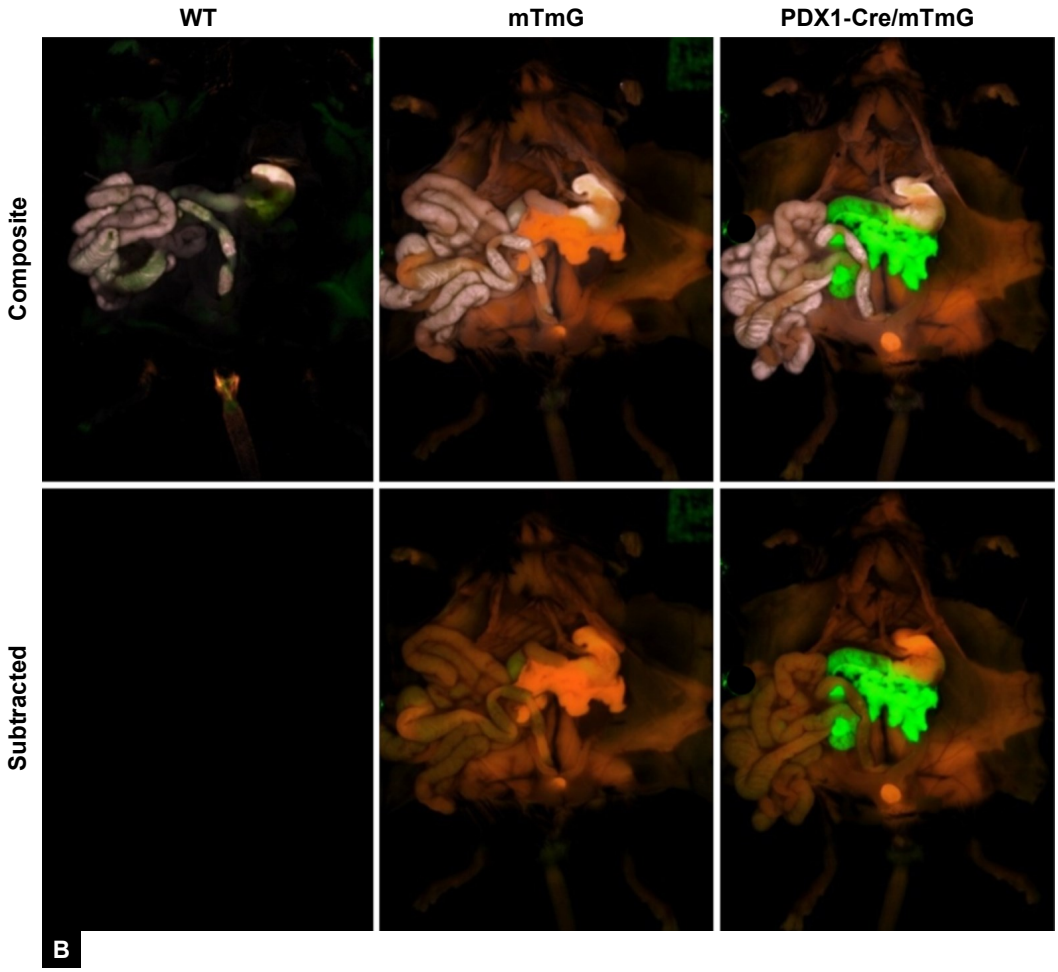

Figure 3. Expression patterns of tdTomato and EGFP; gross anatomical imaging and findings of the PDX1-Cre/mTmG mouse model, Continued

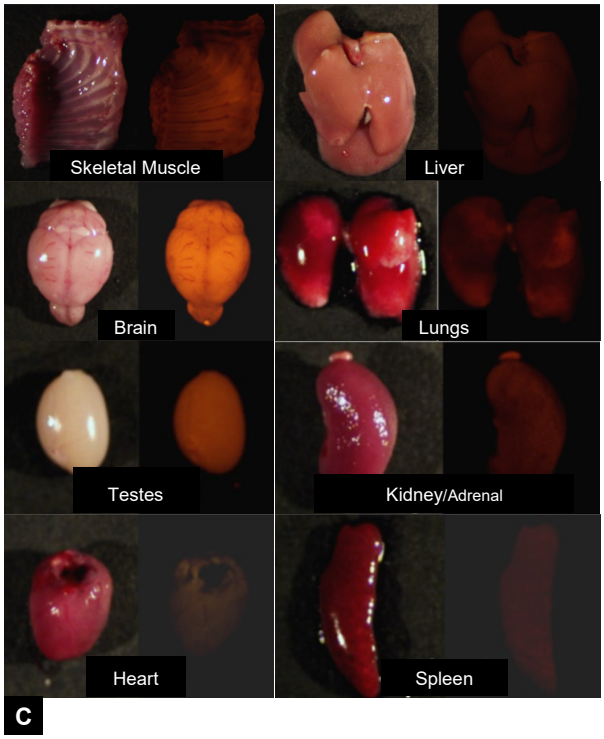

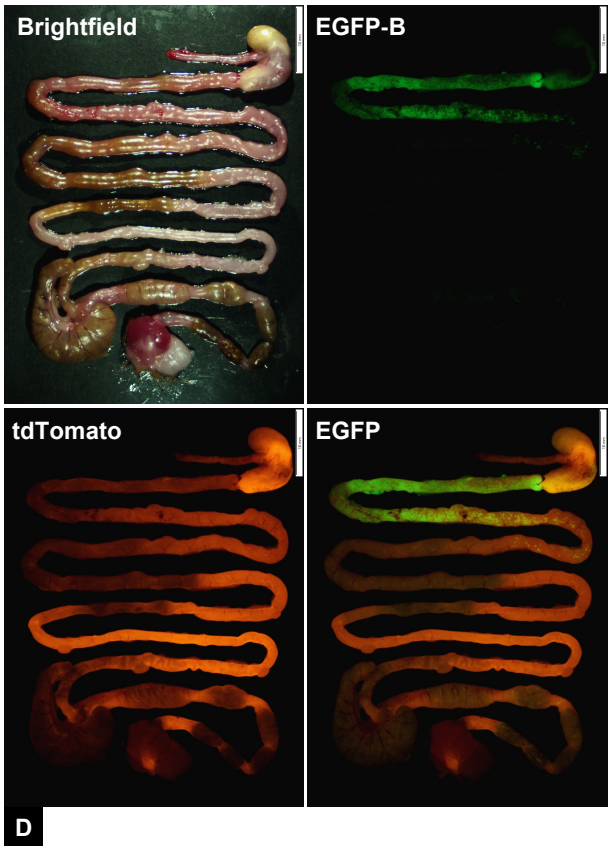

Figure 3. Expression patterns of tdTomato and EGFP; gross anatomical imaging and findings of the PDX1-Cre/mTmG mouse model, Continued

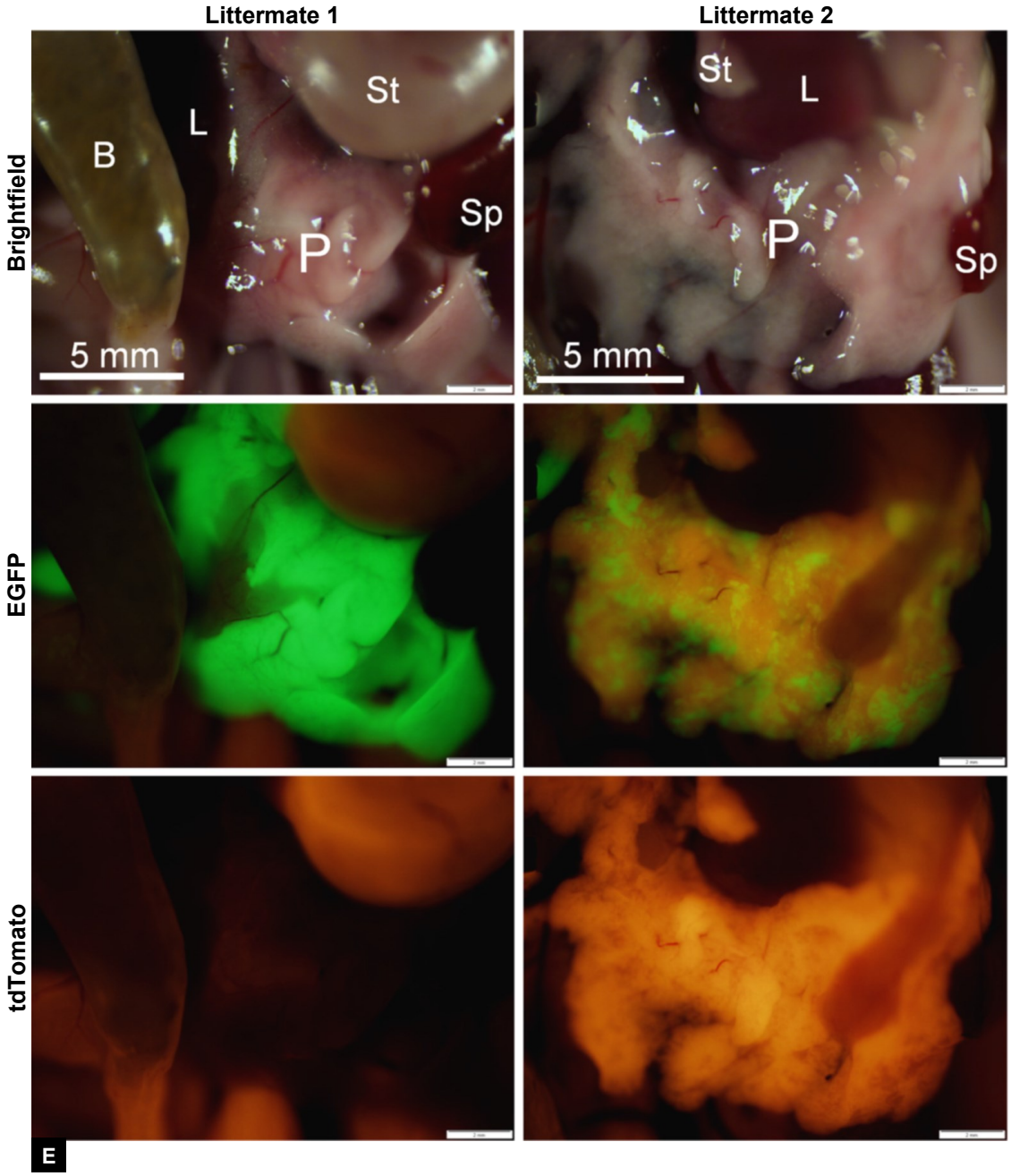

Figure 3. Expression patterns of tdTomato and EGFP; gross anatomical imaging and findings of the PDX1-Cre/mTmG mouse model, Continued

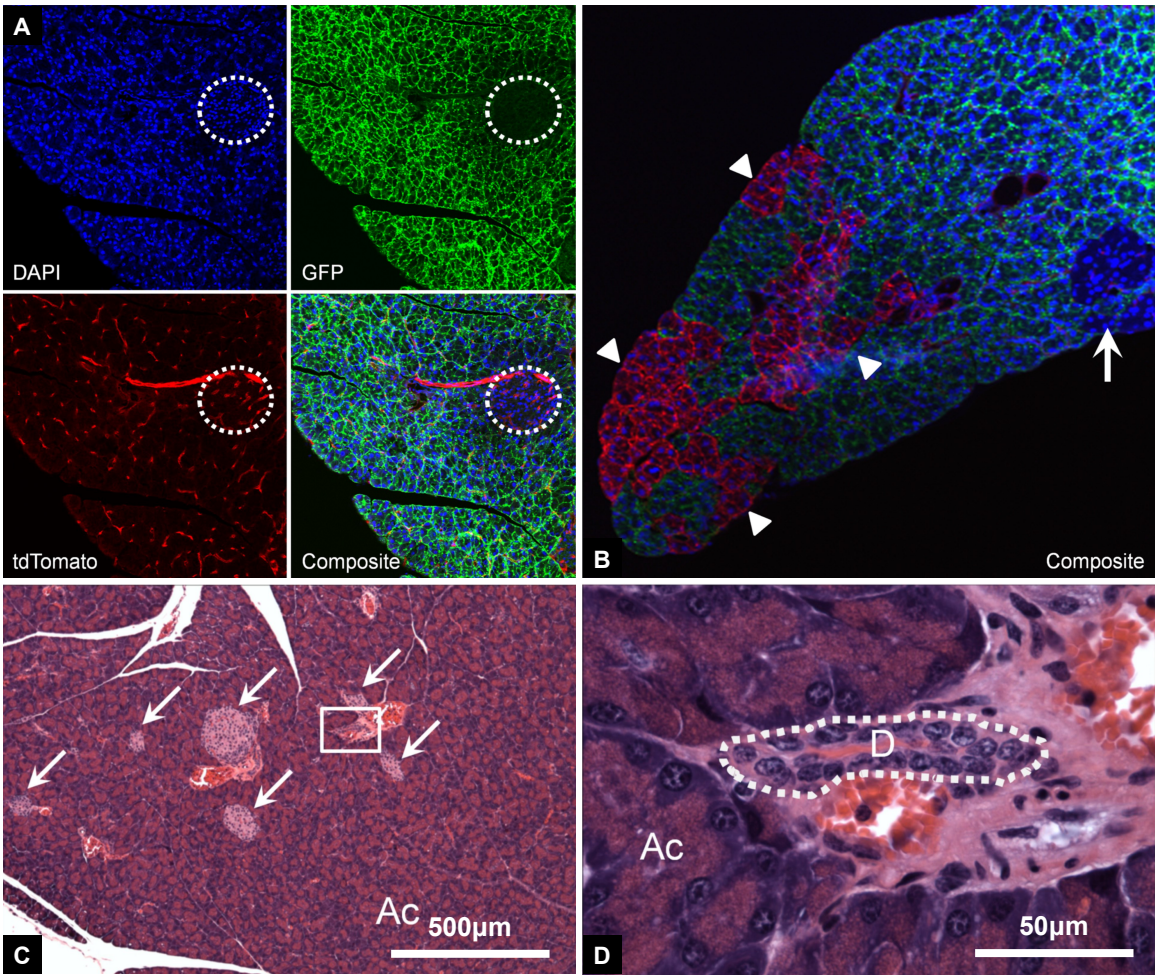

Figure 4. Fluorescence microscopy of frozen and hematoxylin and eosin-stained paraffin-embedded sections of PDX1-Cre/mTmG pancreata detailing the pancreatic microenvironment. A, Section of a pancreas from a PDX1-Cre/mTmG mouse with DAPI-counterstained nuclei and imaged with a confocal microscope collecting DAPI, tdTomato, and EGFP fluorescence channels. EGFP-expressing acinar cell membranes appear bright green. The dashed circle indicates the presence of a pancreatic islet; these cells express EGFP but are relatively faint compared to EGFP expression of acinar cells. Pancreatic stroma (fibroblasts and vasculature) present with bright tdTomato expression. The relatively thick red strand in the upper right quadrant of the tdTomato and composite channels is a small blood vessel. **B**, Wider composite view of a pancreas under the same conditions as **4A**; this view reveals low levels of genetic mosaicism characterized by the presence of irregular clusters of acinar cells expressing tdTomato (white arrowheads) set against the more typical EGFP-expressing pancreatic acinar cell phenotype. These occasional tdTomato-expressing acinar cell islands were found with some frequency in PDX1-Cre/mTmG pancreata. A small intrapancreatic lymph node is indicated by a white arrow. **C**, Hematoxylin and eosin stained section of a PDX1-Cre/mTmG pancreas with normal appearance. Per a typical pancreas, acinar cells (Ac) are predominant interspersed with pancreatic islets (white arrows). The boxed region is enlarged in **4D**. **D**, High magnification view of a pancreatic duct (D, white dashed outline) and adjacent vascular tissue.

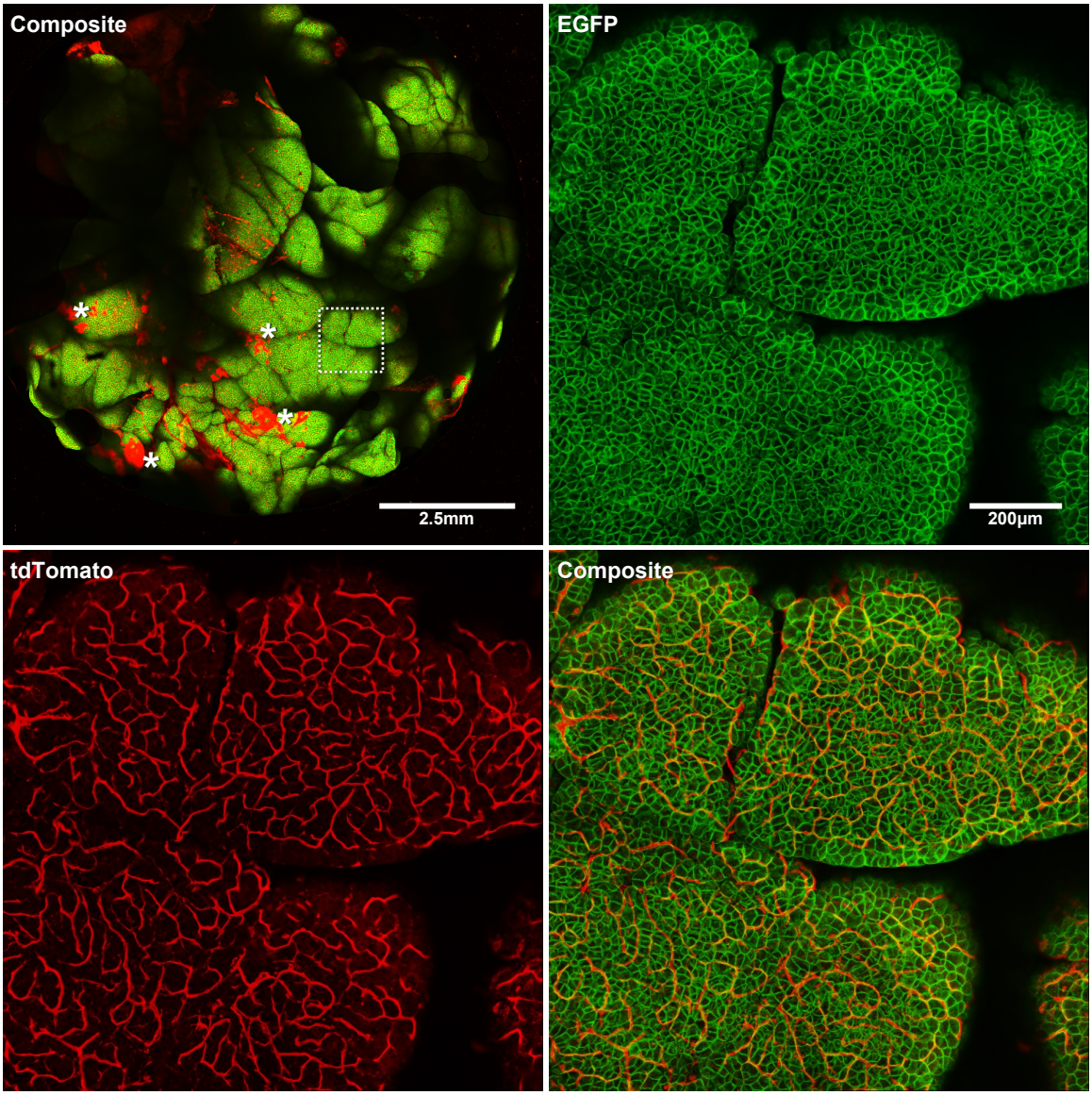

Figure 5. Fluorescence microscopy of a paraformaldehyde-fixed whole pancreas and pancreatic microenvironment of the PDX1-Cre/mTmG mouse. After fixation for 12 hours in low-concentration paraformaldehyde a whole PDX1-Cre/mTmG pancreas was reservoir-mounted and imaged with a Nikon A1R confocal microscope in FITC (EGFP) and Texas Red (tdTomato) channels. The whole-pancreas composite is approximately 9mm in diameter; clearly visible features include the discrete extensions of pancreatic lobes (differentiated by dark borders), vascular structures, and tissue mosaicism (asterisks). The dashed box indicates the selection enlarged in the remaining panels; all high-magnification panels are standard-deviation projections of the tissue section 30µm in total depth in a region approximately 1.36mm^2. EGFP is strongly expressed and highly visible in acinar cell membranes. Three-dimensional stromal structures (fibroblasts and vasculature) are particularly evident and appear uninterrupted due to the imaging depth and projection method. This method of fixation and imaging yields significantly more vibrant and sharper images than previous imaging methods and permits excellent three-dimensional visualization of the tissue.

Figure 6. Fluorescence microscopy of PDX1-Cre/mTmG mouse bowel sections detailing the small intestine and colon microenvironments. Tissue samples were fixed for 12 hours in low-concentration paraformaldehyde and imaged with a Nikon A1+ multiphoton microscope (**A**, **B**) or Nikon A1R confocal microscope (**C**). **A**, Detail of the duodenal microenvironment in FITC (EGFP), Texas Red (tdTomato), and DAPI (Collagen) second-harmonic channels 194μm in total depth; the bottom four panels are at a tissue depth of 58μm. Both longitudinal and circular smooth muscle layers of the muscularis externa, vasculature, and connective tissue (collagen) are observable from this imaging series. Submucosal glands are evident in this small section but cannot be reliably identified without markers in addition to fluorescence; irregularity of EGFP expression was expected. tdTomato-expressing epithelial cells (no PDX1 expression) lie adjacent to PDX1-expressing cells in the mucosa; due to the intensity of tdTomato in the membrane-rich muscularis externa these cells appear dim; however, they are still present. **B**, Cross section of the duodenum, prepared and imaged as in **A**. A wide range of features may be observed; villi, crypts, and the muscularis externa are the most prominent features. The outermost epithelial layer of villi exhibit typical columnar morphology; goblet cells are evidenced by their large diameter and distribution throughout the villi. Vasculature and lacteals may be seen in internal structures of villi, predominantly on the right half of the whole-cross section panels. Per known expression patterns of PDX1, not all duodenal villus epithelium exhibit EGFP expression. **C**, Microenvironment detail of the proximal large intestine wall prepared in the “Swiss Roll” method; imaged under FTIC (EGFP) and Texas Red (tdTomato) channels. The muscularis is highly visible throughout the tissue section as a thick band with strong tdTomato expression; in addition, the muscularis mucosae is also visible as a thin red band at the base of the mucosa throughout the tissue. The proximal colon exhibits mucosal folds; the lamina propria is clearly visible within the mucosal folds. Crypts are less apparent but can be observed in some areas. The selection panel shows a region with some minor clusters of EGFP expression; PDX1 expression in the colon is minimal during normal development. Regions with PDX1 activity maintain normal colon epithelium morphology.

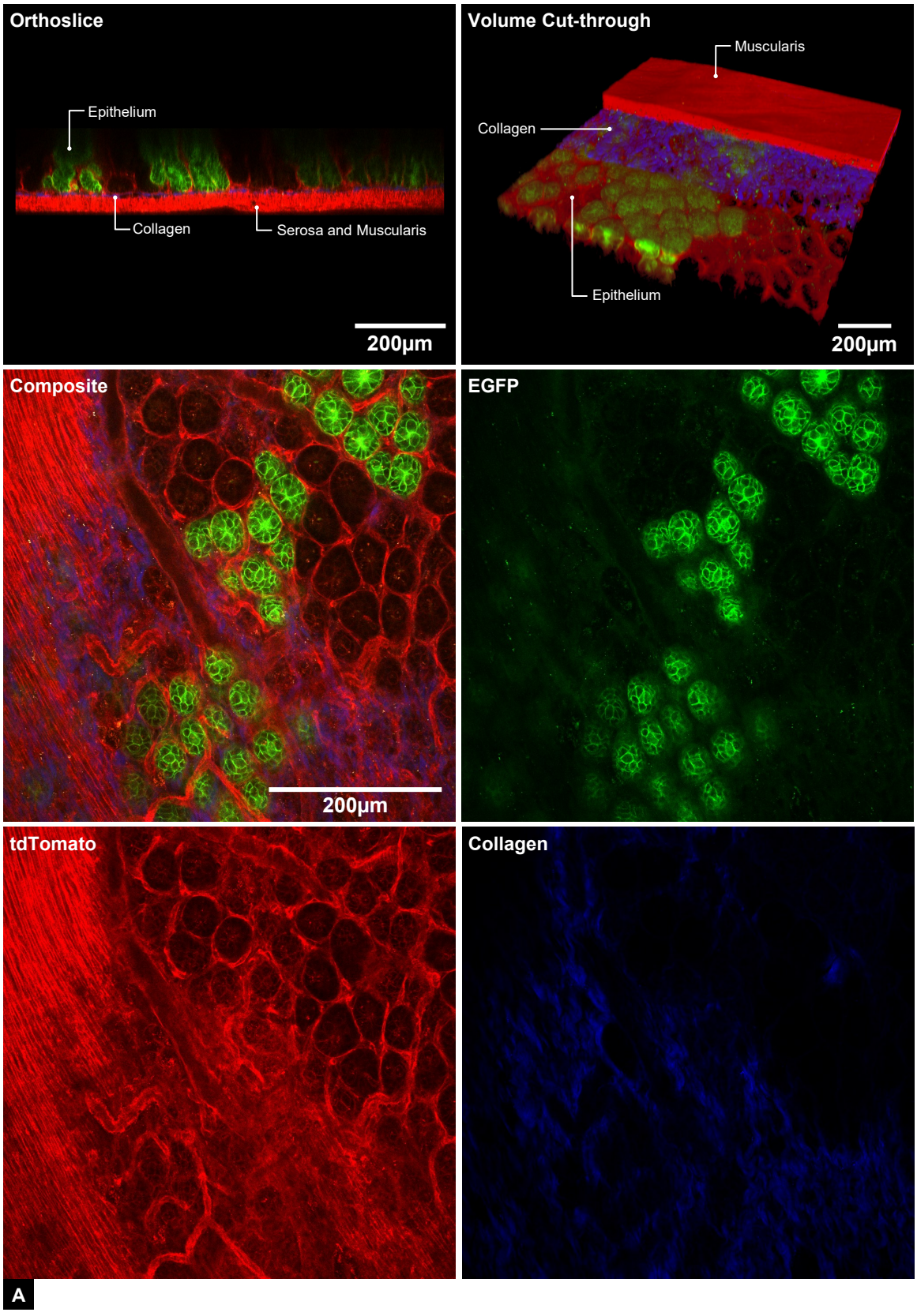
Orthoslice
Epithelium
Collagen
Serosa and Muscularis
200µm
Volume Cut-through
Muscularis
Collagen
Epithelium
200µm
Composite
200µm
EGFP
tdTomato
Collagen
A

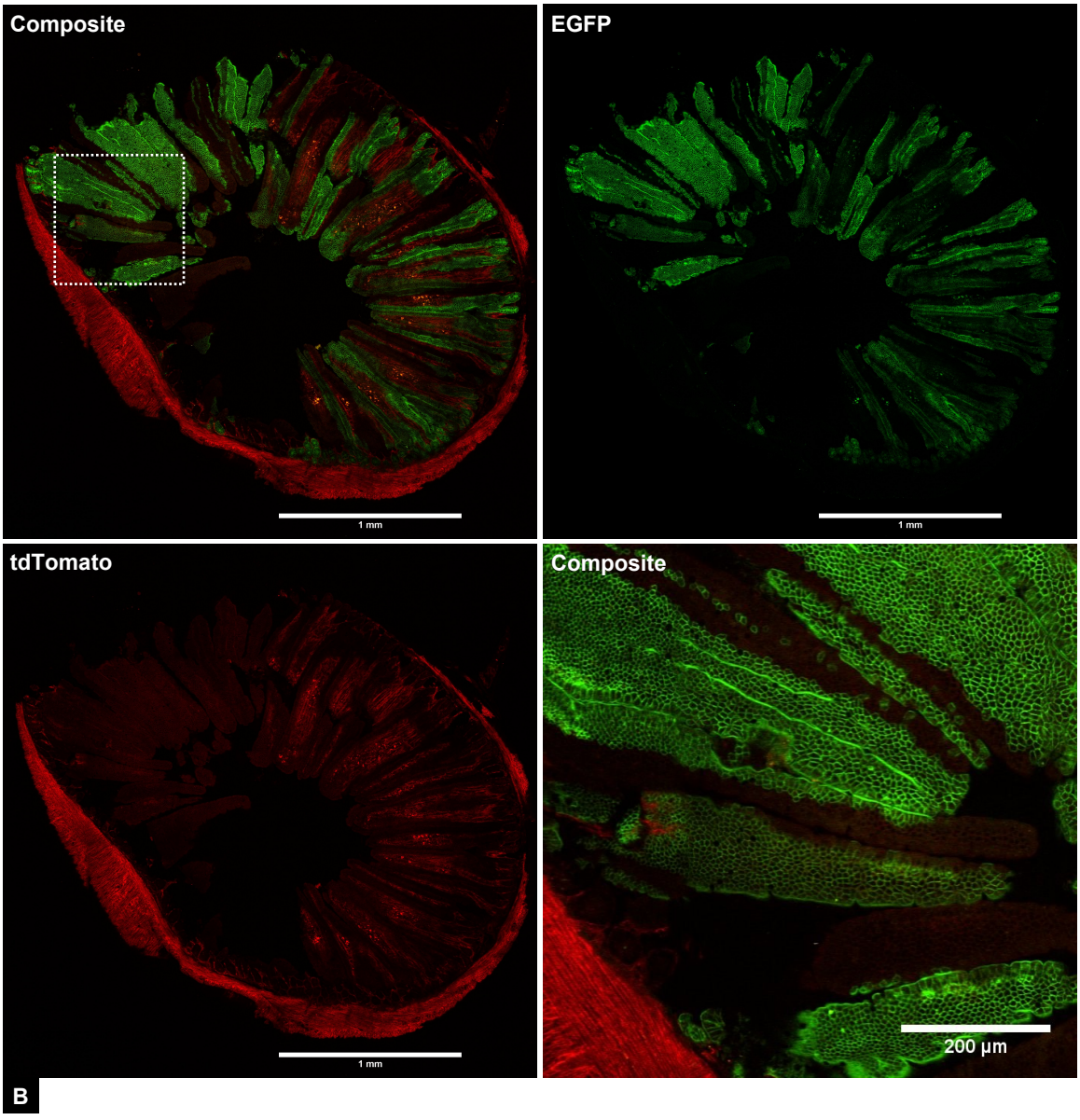

Figure 6. Fluorescence microscopy of PDX1-Cre/mTmG mouse bowel sections detailing the small intestine and colon microenvironments, Continued

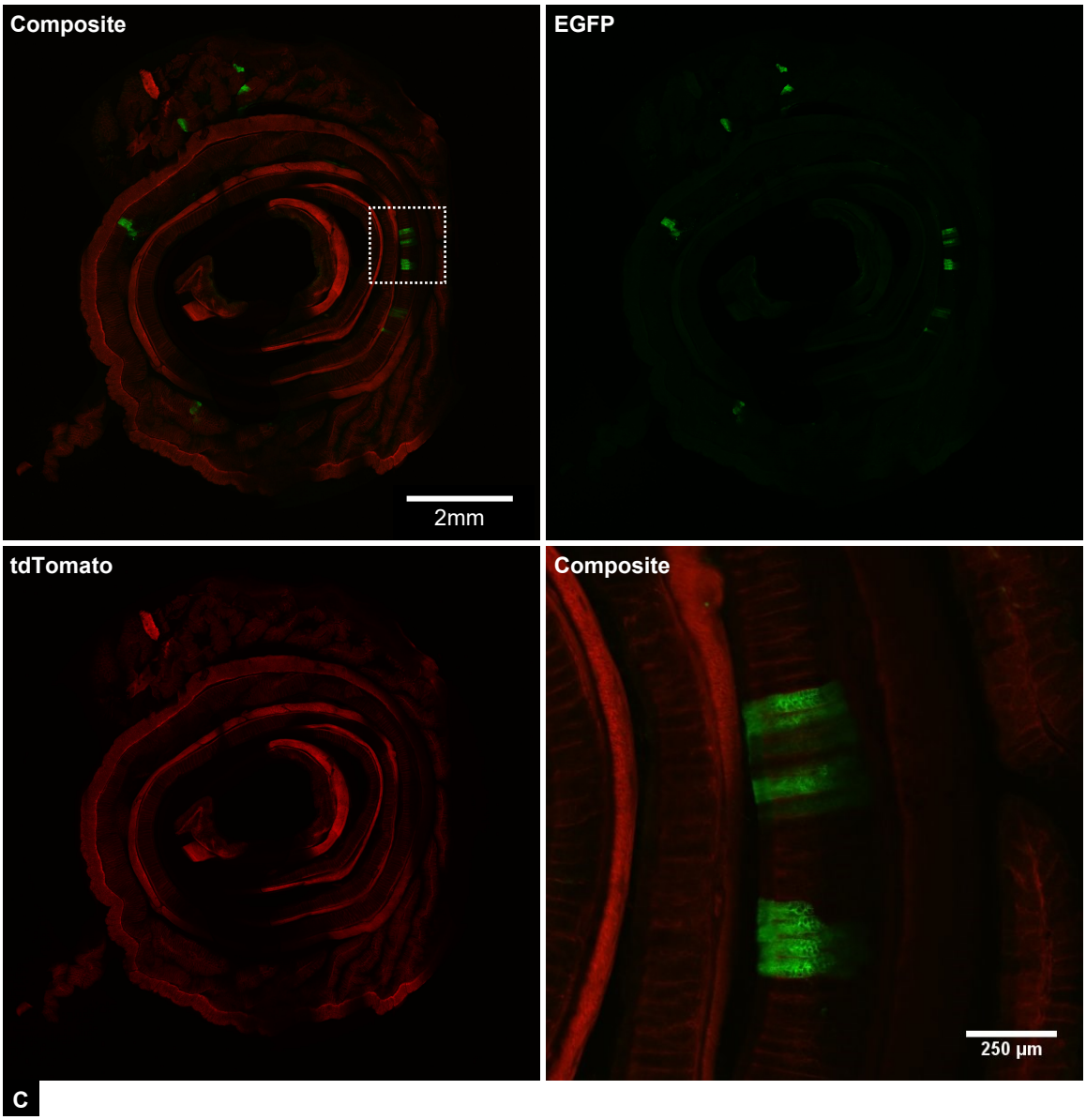

Figure 6. Fluorescence microscopy of PDX1-Cre/mTmG mouse bowel sections detailing the small intestine and colon microenvironments, Continued

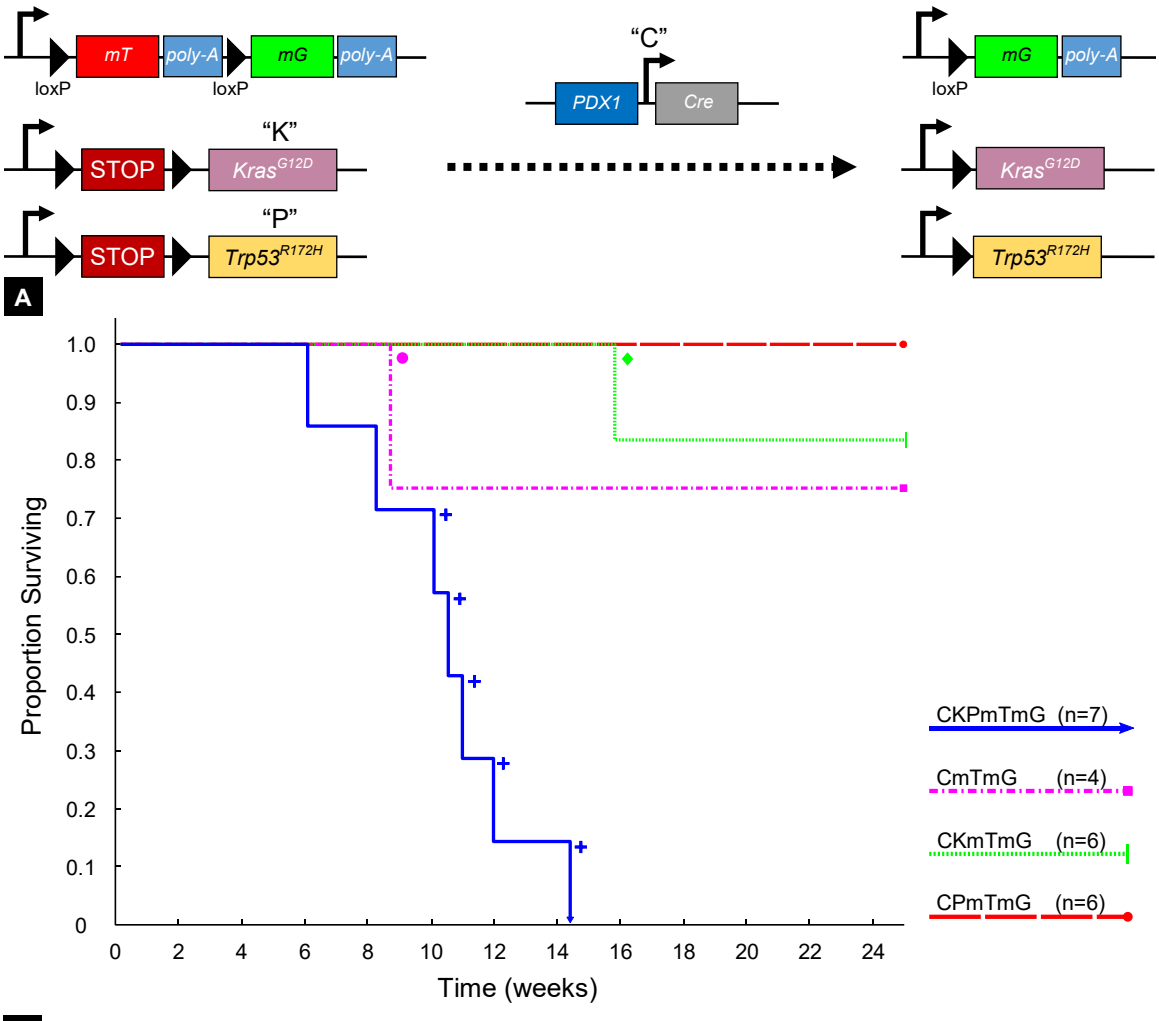

Figure 7. Characteristics and design of the PDX1-Cre^{+}/Kras$^{G12D/+}$/Trp53$^{R172H/+}$/mTmG^{+} mouse model. This model is also abbreviated to CKPmTmG from PDX1-Cre^{+} ("C"), Kras$^{G12D/+}$ ("K"), and Trp53$^{R172H/+}$ ("P"); mTmG is described previously (Figure 1). Mice which lack any of the four transgenes described drop the respective letter from their abbreviation. **A**, Diagram of the four transgenes of the CKPmTmG mouse model before and after rearrangement by PDX1-Cre. Wild type alleles of Kras and Tp53 are present and functional before and after recombination by PDX1-Cre. **B**, Kaplan-Meyer survival chart of four relevant genotypes: quadruple transgenic CKPmTmG (n=7) mice, triple transgenic CKmTmG (n=6) and CPmTmG (n=6) mice, and double transgenic CmTmG (n=4) control mice. All CKPmTmG mice died spontaneously or were euthanized with high morbidity and significant tumor burdens; in the remaining three groups mice were euthanized for imaging as controls or morbidity due to causes unrelated to tumor burden. +, mice euthanized due to morbidity; ●, mice euthanized as healthy controls; ♦, mice euthanized due to fight wounds.

Figure 8. **Fluorescence imaging and histology of the CKPmTmG mouse model. A**, Olympus OV100 brightfield and fluorescence imaging of the CKPmTmG mouse model and its sub-genotypes; as with the PDX1-Cre/mTmG mouse model, tdTomato expression is ubiquitous. Patterns of EGFP expression vary by genotype; the greatest predictor of expanded EGFP expression is presence of the $Kras^{G12D/+}$ allele. Solid and semi-solid pancreatic masses exhibit greater tdTomato expression than unaffected pancreata. White arrows indicate pancreata; white asterisks indicate pancreatic masses. Luminesce cures of brightfield images were mildly adjusted to account for changes to the brightfield illumination arms of the Olympus OV100; no other changes were made. **B-D:** All inset boxes correspond to the row of higher-magnification panels immediately beneath including all associated fluorescence and brightfield channels. **B**, CKPmTmG male mouse euthanized at 74 days of age. Panels **i-iv** show the full abdominal cavity under brightfield and fluorescence channels; the yellow dotted outline indicates the gross pancreas tumor border. This tumor is semi-solid and sits beneath the stomach, duodenum, and remaining pancreas. Panels **v-vii** show a magnetified view of this tumor. The EGFP channel makes apparent a surface covered by distorted and distended EGFP-expressing pancreatic ducts and duct-like structures. Magnification of the abnormal duct structures increases in panels **viii-xi**. Panels **xii-xiii** are paraffin-embedded, hematoxylin and eosin stained sections of the pancreas and pancreatic tumor. These sections show replacement of acini and encroachment upon islets (dashed circle, **xii**) by atypical ducts (arrows, **xii**) with features of PanIN. Widespread ductal atypia (dashed circle, **xiii**) with focal luminal necrosis of ducal epithelium (arrowhead, **xiii**). **C**, CKPmTmG male mouse euthanized at 104 days of age. Panels **i-iii** detail the pancreatic tumor of this mouse under brightfield and fluorescence channels. This tumor is composed of serous cystic masses interspersed among acinar tissue atrophy. Panels **iv-viii** are paraffin-embedded, hematoxylin and eosin stained sections of this tumor. Multiple features of PanIN may be observed; these include papilliform (**iv**, dashed line), cribriform (**v**, dashed oval), ductal atypia and duct-centered desmoplasia (**vi**) leading to progressive isolation of islets (**viii**, dashed circle). **D**, CKPmTmG female mouse euthanized at 84 days of page. Panels **i** and **ii** show this tumor under brightfield and EGFP-fluorescence channels; cystic and solid regions of this tumor are immediately observable. Panel iii shows a cross section of this entire pancreas and tumor at low magnification; boxes indicate the magnified regions shown in panels **iv-vi**. Findings include atrophy and replacement of normal acini by proliferation and expansion of atypical ducts and desmoplasia (**iv** and **v**, black arrowheads). Panel **vi** shows a solid region of the tumor with multiple features of high grade malignancy, including nuclear atypia and a high mitotic rate (**vi**, white arrows).

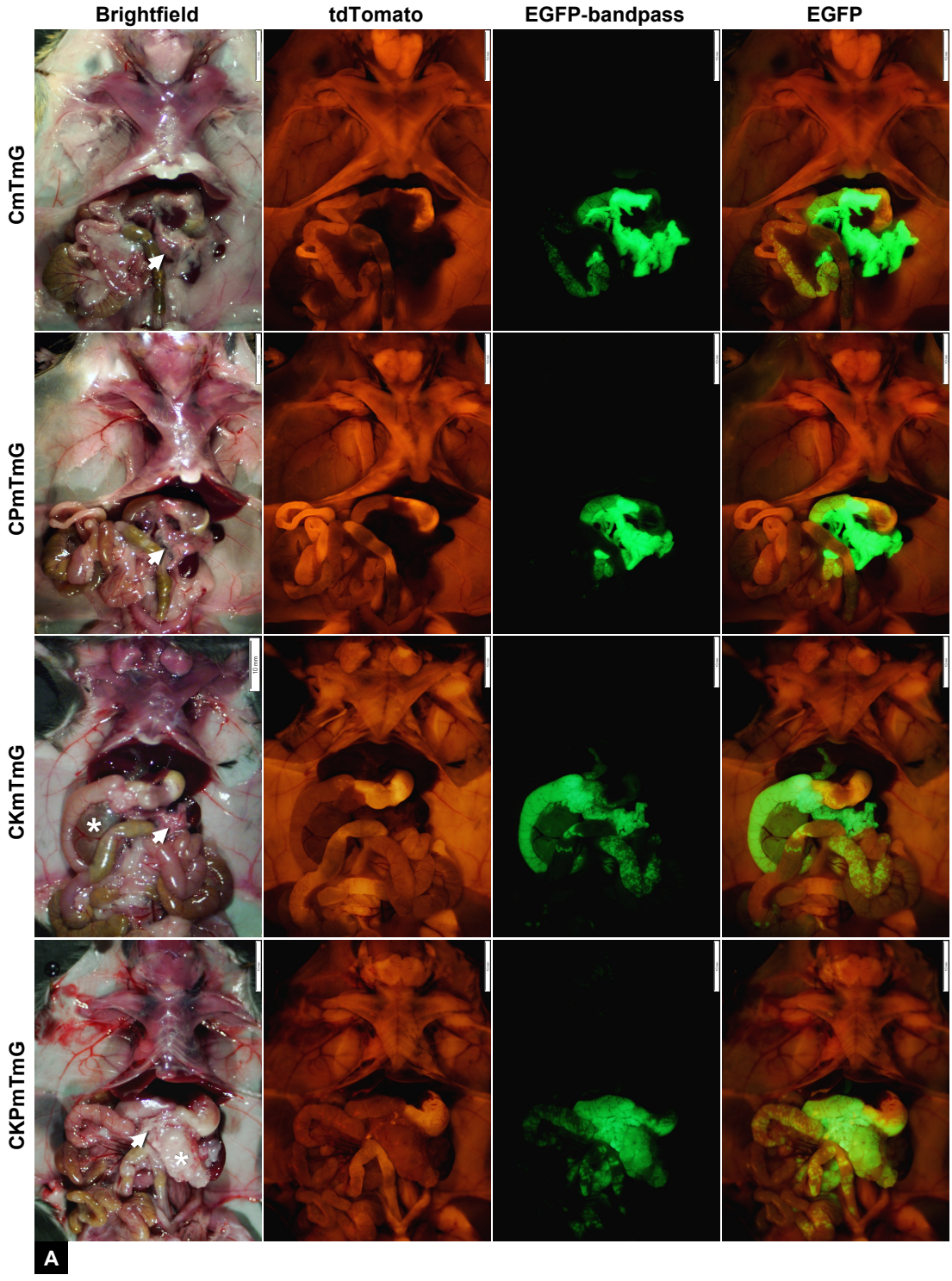
Brightfield
tdTomato
EGFP-bandpass
EGFP
CmTmG
CPmTmG
CKmTmG
CKPmTmG
A

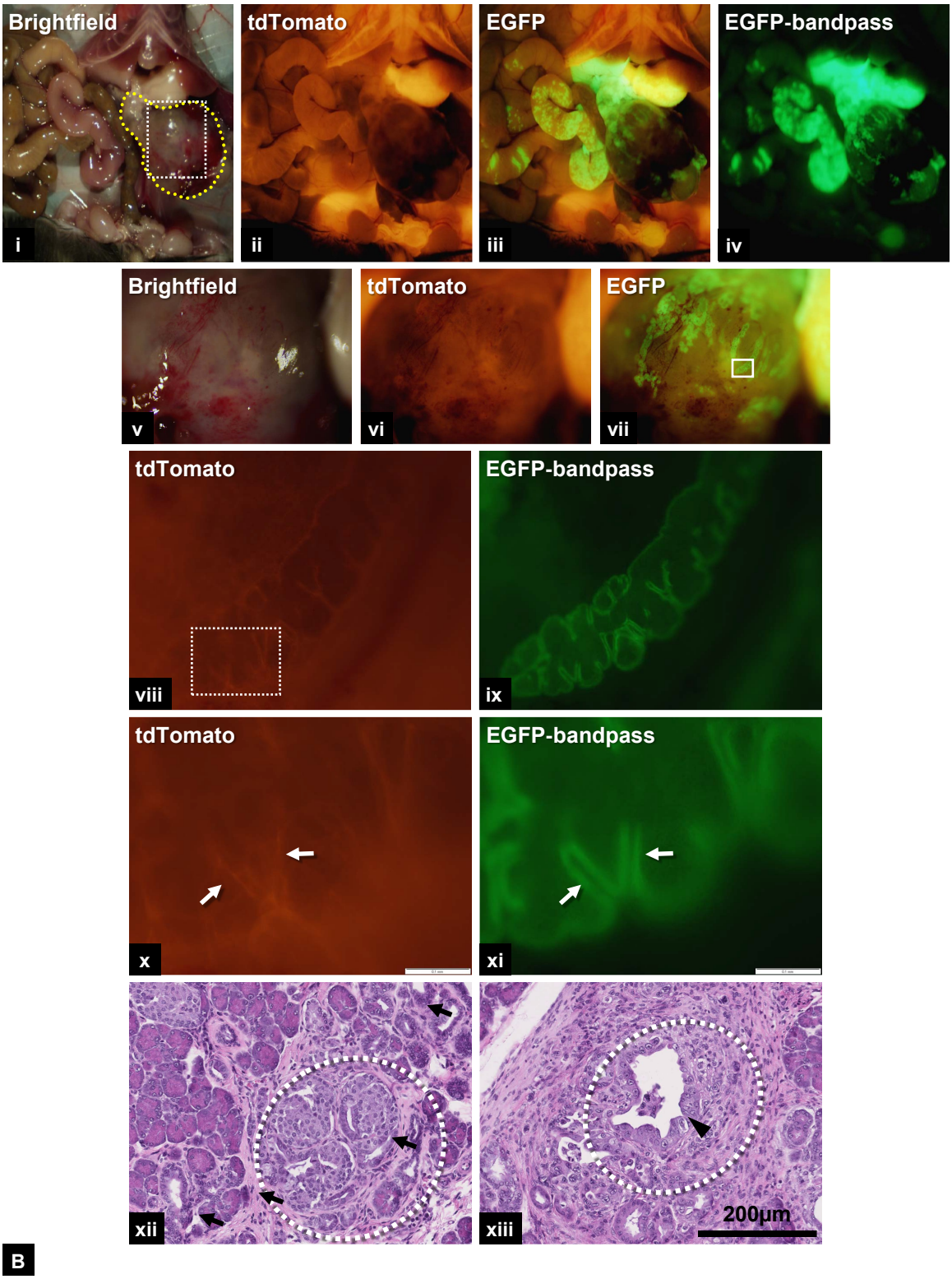

Figure 8. Fluorescence imaging and histology of the CKPmTmG mouse model, Continued

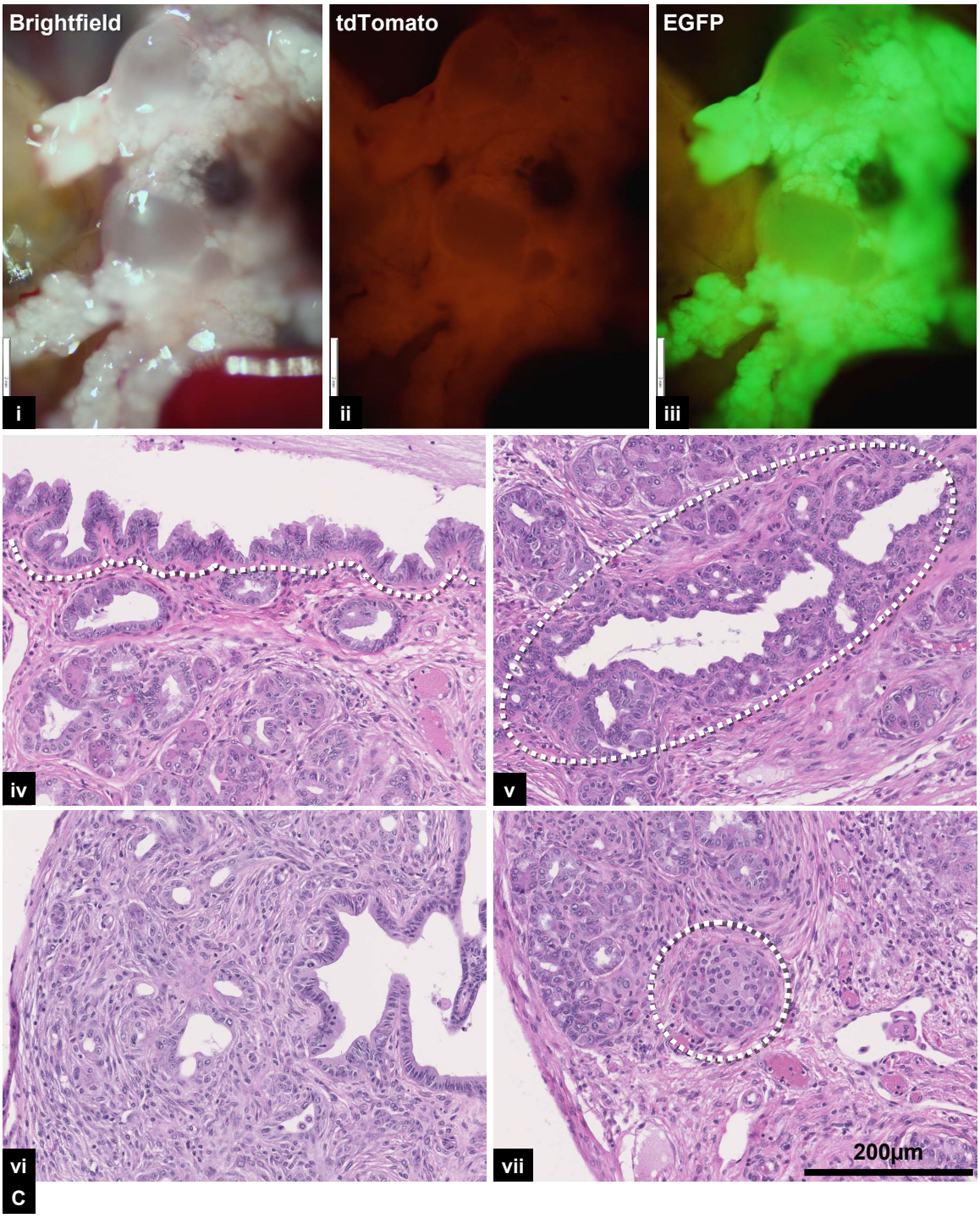

Figure 8. **Fluorescence imaging and histology of the CKPmTmG mouse model**, Continued

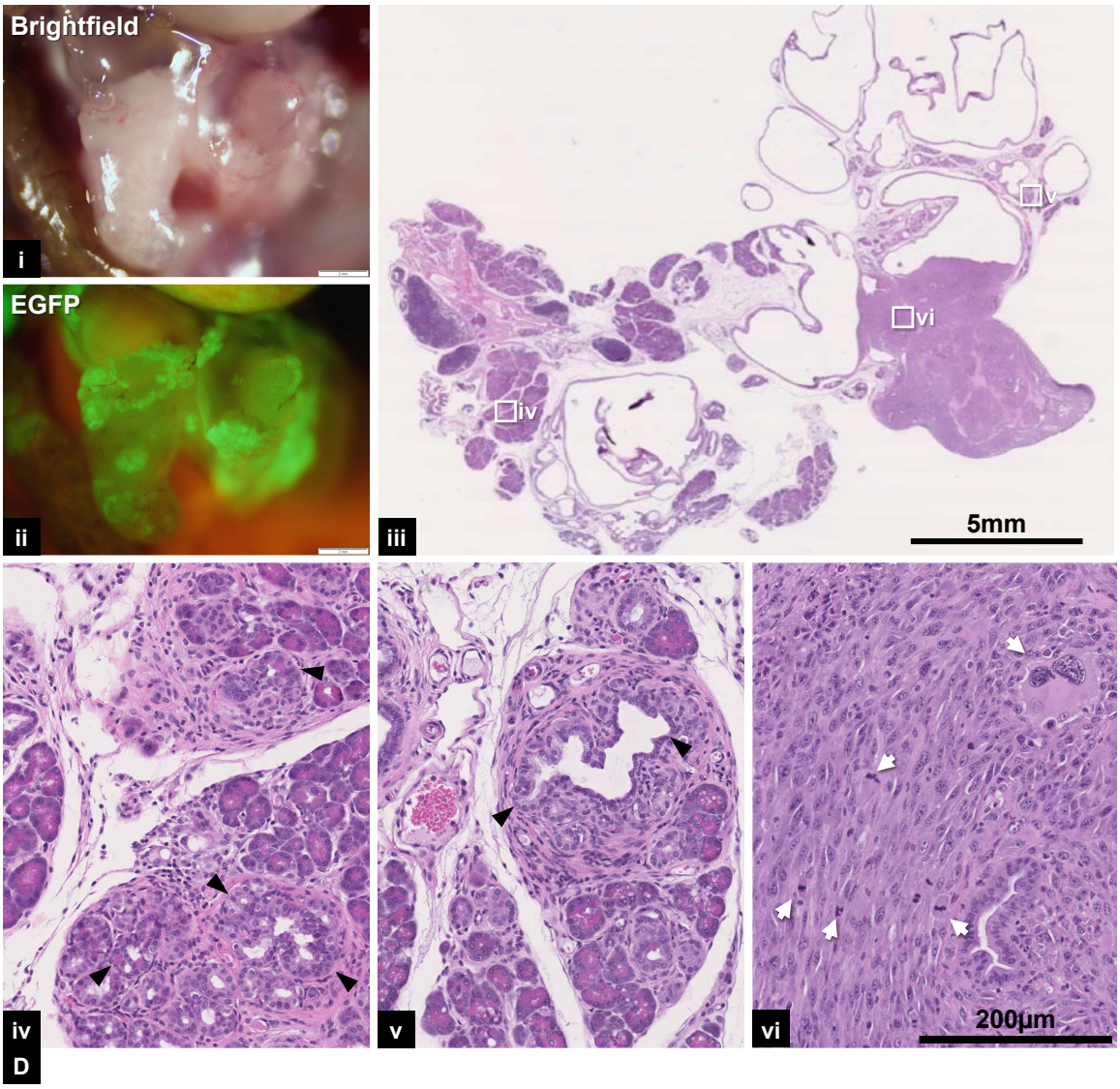

Figure 8. **Fluorescence imaging and histology of the CKPmTmG mouse model**, Continued

Figure 9. Fluorescence microscopy of the CKmTmG whole pancreas and pancreatic microenvironment. Images were acquired after fixation for 12 hours in low-concentration paraformaldehyde; a whole CKmTmG pancreas was reservoir-mounted and imaged with a Nikon A1R confocal microscope in FITC (EGFP) and Texas Red (tdTomato) channels. **A**, The whole-pancreas composite is approximately 9mm in diameter. This pancreas predominantly shows features characteristic of pancreatic ductal intraepithelial neoplasia (PanIN)-1 and some features of PanIN-2; major structures include large cystic areas (dark interior regions with green cell borders), abnormal dilated acinar and ductal clusters (yellow dashed circle), and desmoplasia. Islets appear normal; other features include a large lymphoid aggregates, adipose cells, and vasculature. Isolated lobules of tissue with normal acinar and ductal phenotype indicate rare Cre-recombination failures of the transgenes of interest (see inset panels in **9B**). Selected examples of each structure or characteristic are identified. Dilated acinar clusters and ducts, white circle; cysts, **C**; desmoplasia, **da**; islets, **I**; lymphoid tissue, **L**; adipose cells, **Ad**; major vasculature, **v**. **B**, Inset boxes detail; both insets are approximately 1.38mm^2 and generated from standard deviation projections of tissue (**i-iii** depth: 40.5μm; **iv-vi** depth: 39.0μm). Much of the remaining epithelium of this pancreas has acquired a columnar phenotype; this trait is particularly evident along the borders of cystic regions of the tissue. Additionally, the epithelium is far less dense than is observed in a pancreas lacking the Kras^{G12D} transgene, indicating widespread acinar cell atrophy. Desmoplasia is particularly noticeable in the tdTomato channel; pancreas microvasculature have proliferated and become highly disordered. Panels **i-iii** exhibit a dilated duct and acinar cell “branch” (center) and examples of Cre-recombination failure; these include a lobule of tdTomato-expressing acinar cells with EGFP-expressing ducts (upper center) and a lobule of EGFP-expressing acinar cells with a normal phenotype and normal stroma (upper right). A dotted arc labels cells with papilliform morphology typical of PanIN-1B. Panels **iv-vi** contain islets with normal appearance. Selected examples of each structure or characteristic are identified. Cysts, **C**; dilated acinar clusters, **a**; ducts, **dt**; desmoplasia, **da**; islets, **I**; lymphoid tissue, **L**; adipose cells, **Ad**; Cre-recombination failures, *****.

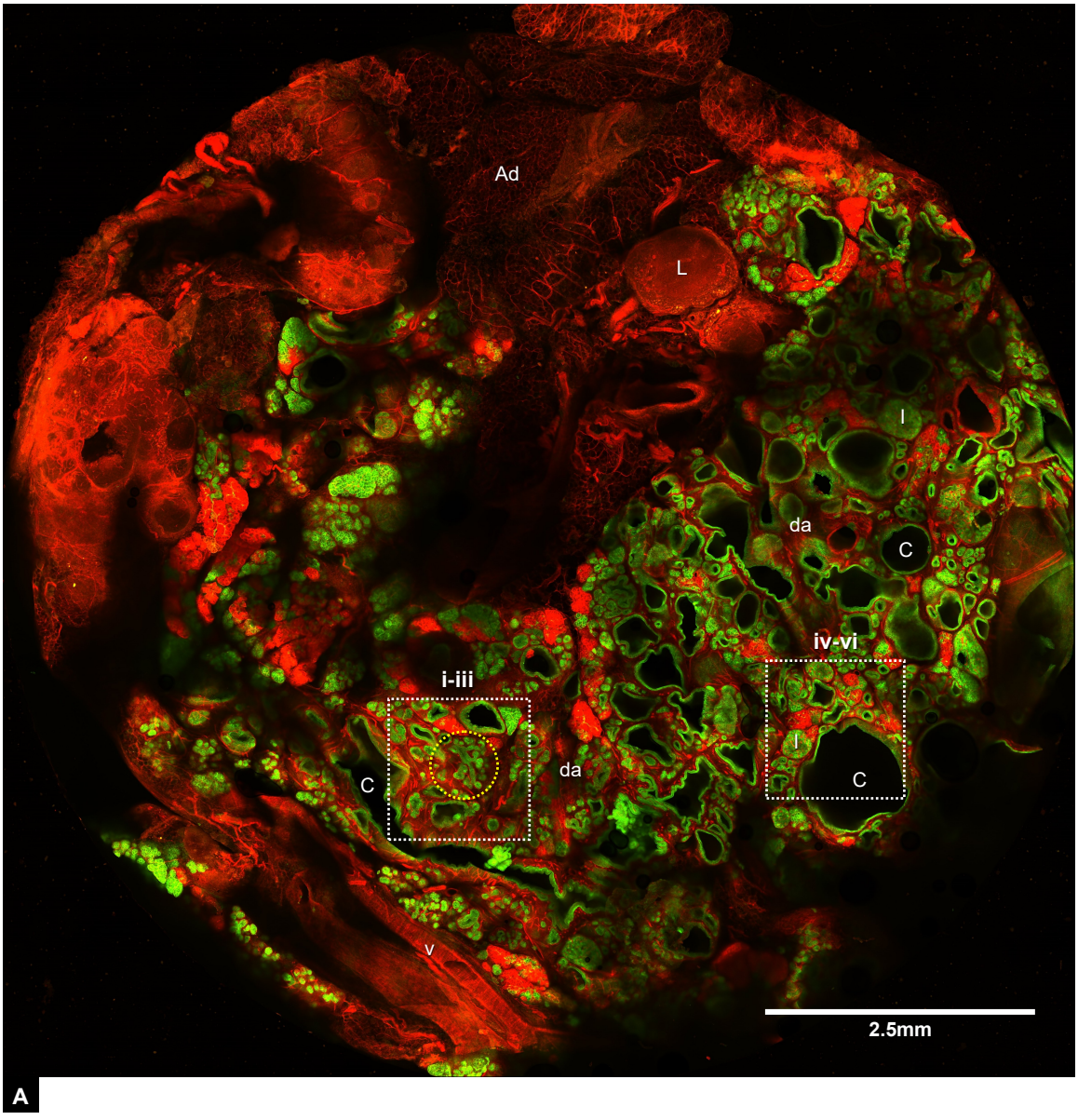
Ad
L
l
da
C
iv-vi
i-iii
l
C
C
da
v
2.5mm
A

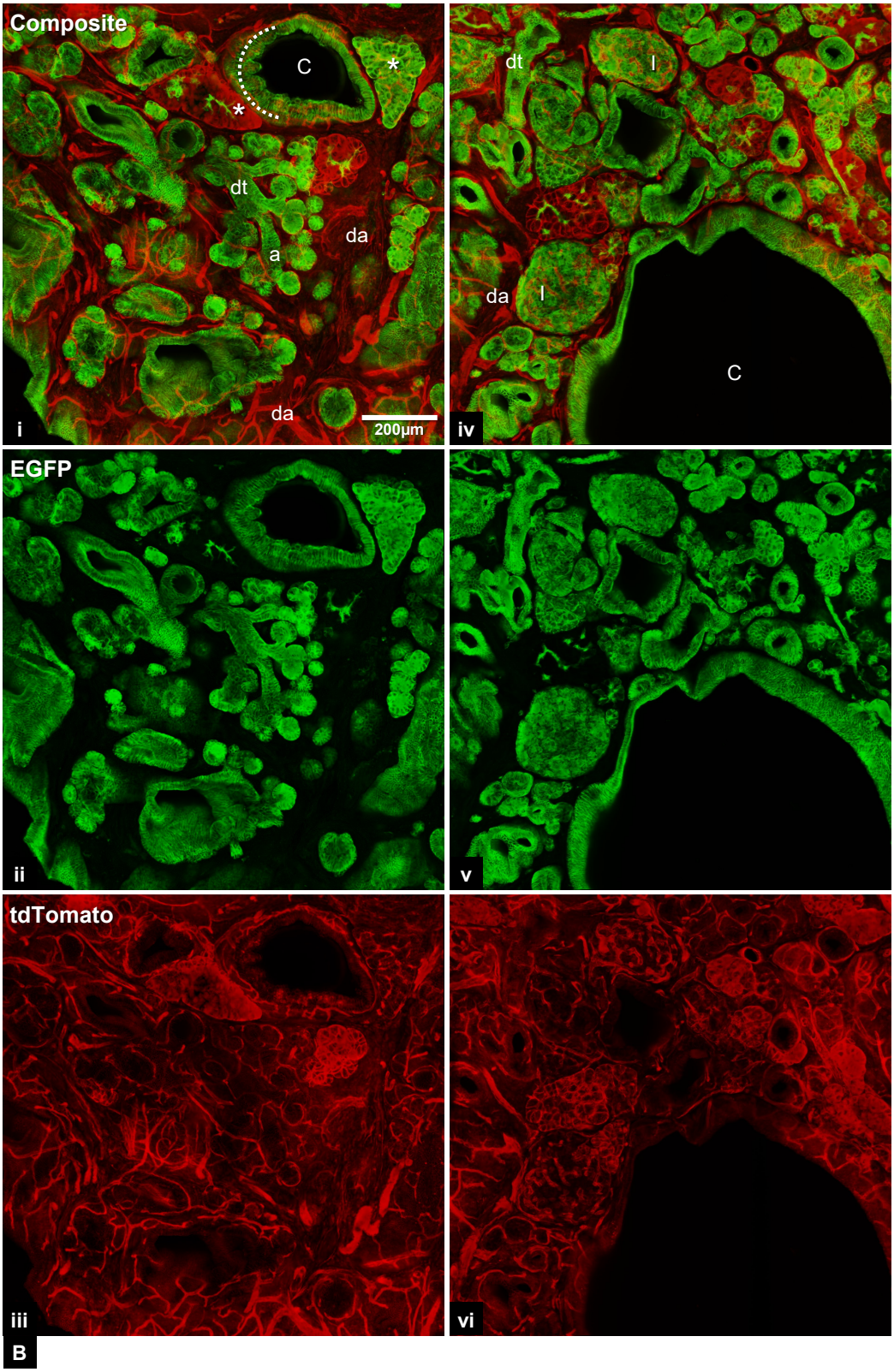

Figure 9. Fluorescence microscopy of the CKmTmG whole pancreas and pancreatic microenvironment, Continued

Figure 10. Distribution of EGFP throughout the gastrointestinal tract by genotype. The gastrointestinal tracts of mice of four genotypes were collected and analyzed; genotypes of interest are CmTmG, CPmTmG, CKmTmG, and CKPmTmG mice. Tissues were imaged via the OV100 and analyzed in Fiji/ImageJ. **A**, EFGP-bandpass images of gastrointestinal tracts (esophagus to anus) of mice from the four relevant genotypes. In mice bearing the activated $Kras^{G12D}$ allele, EGFP is detected further down the duodenum and in the cecum and large intestine. **B**, Statistical analysis of EGFP distributions in the gastrointestinal tracts of these four genotypes; **n=7** in all groups. ANOVAs with Bonferroni post-hoc ranking were performed with MaxStat Lite. No differences were observed in overall bowel length; all other metrics showed at least one statistically significant difference between groups. Activated $Kras^{G12D}$ is the greatest predictor of an observable change in phenotype.

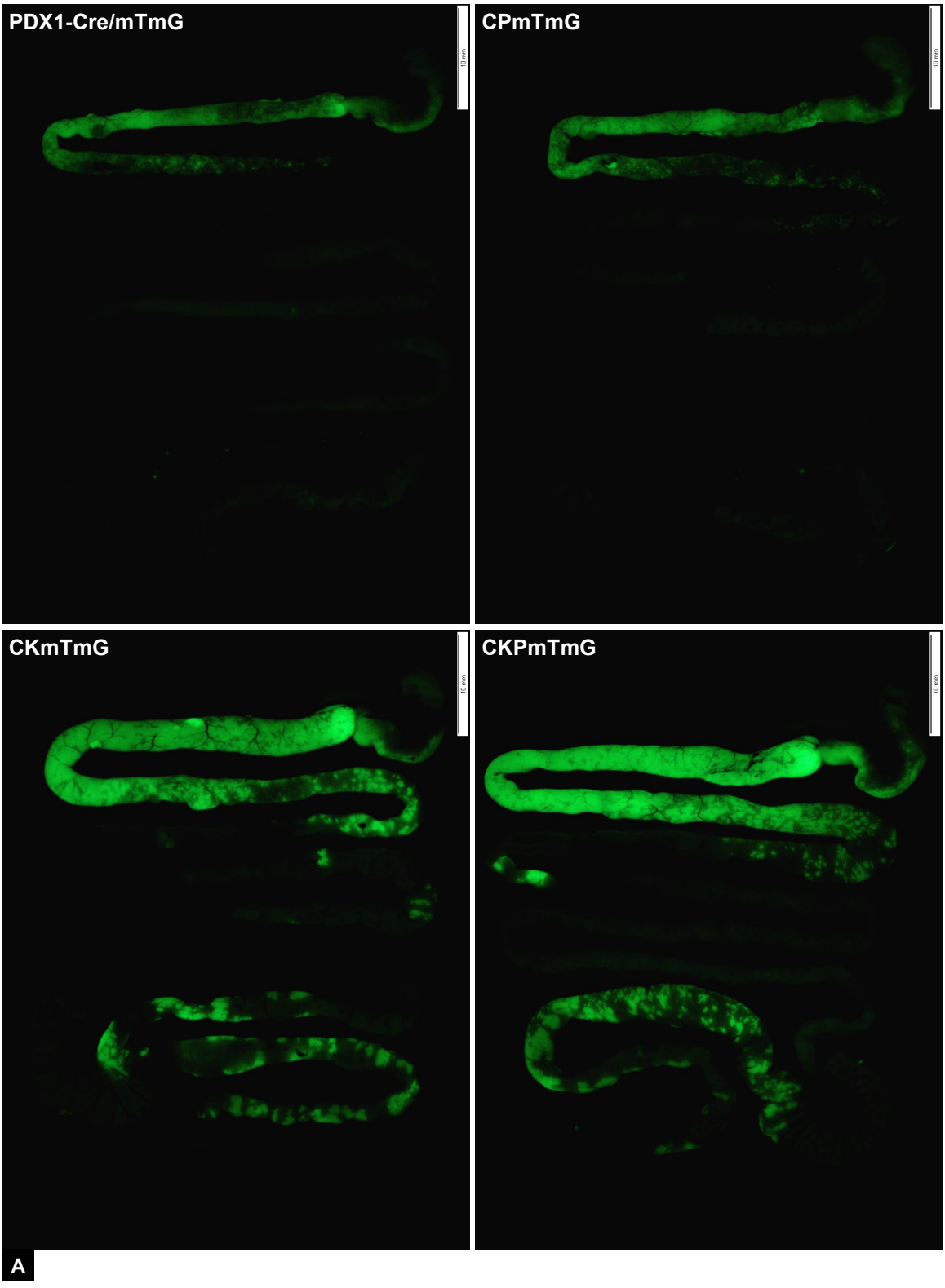
PDX1-Cre/mTmG
CPmTmG
CKmTmG
CKPmTmG
A

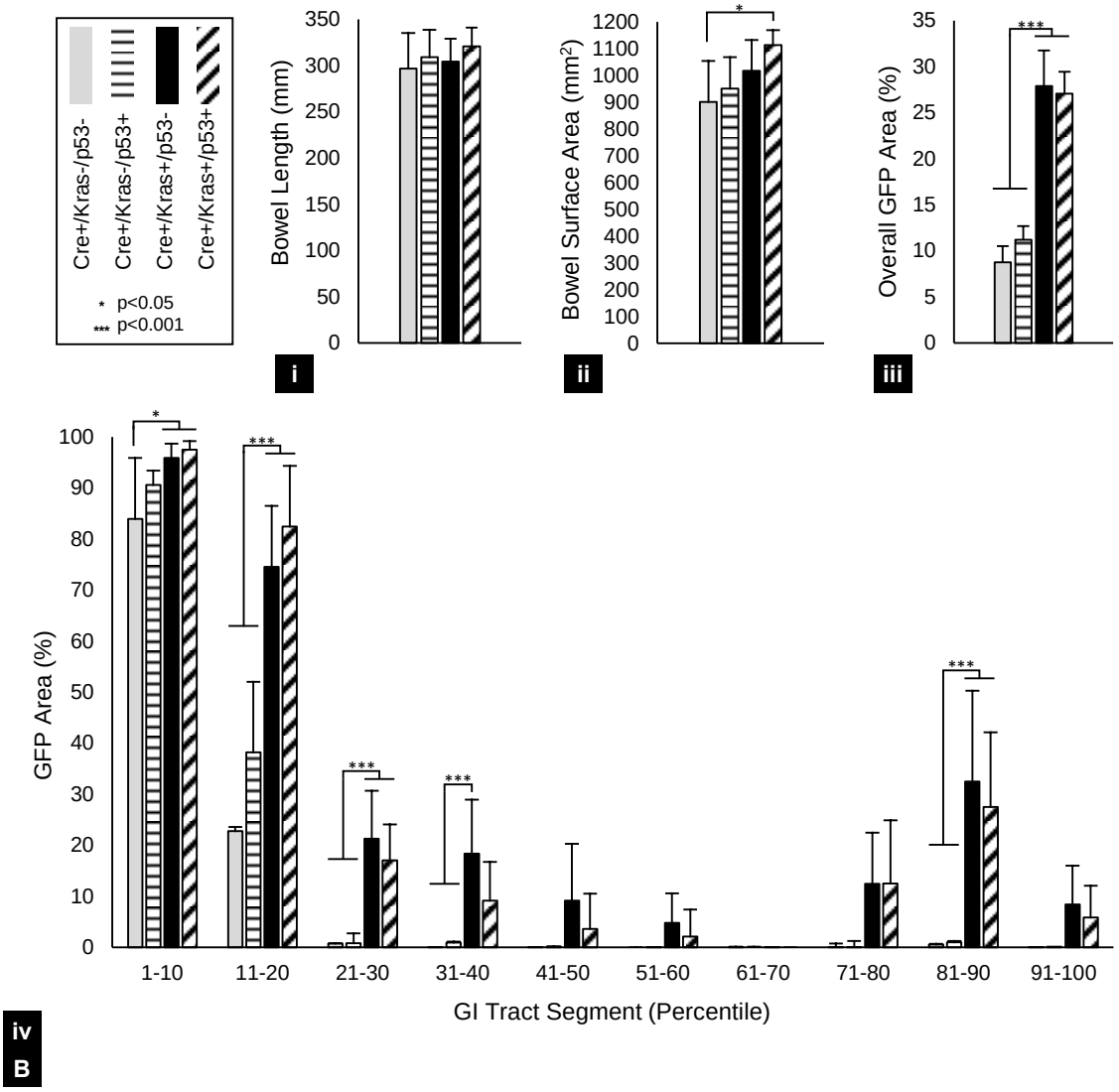

Figure 10. Distribution of EGFP throughout the gastrointestinal tract by genotype, Continued

Figure 11. Histology and fluorescence microscopy of the CKmTmG large intestine microenvironment. Tissue samples were prepared via the “Swiss Roll” method. **A**, Images of this cecum and proximal large intestine wall were acquired in FTIC (EGFP) and Texas Red (tdTomato) channels after overnight fixation in paraformaldehyde. As with its $Kras^{G12D}$-counterpart, the muscularis is highly visible throughout the tissue section as a thick band with strong tdTomato expression and the muscularis mucosae is also apparent throughout the tissue. All typical features of the large intestine wall appear normal; these include mucosal folds with columnar epithelium, lamina propria, and crypts. Of note are the large regions of EGFP-expressing epithelium; despite the presence of cells with apparent Cre-mediated recombination, there are no cells with obvious abnormalities. This effect was observed only to this magnitude in mice with activated LSL-$Kras^{G12D}$. **B**, Paraffin-embedded hematoxylin and eosin stained cecum and large intestine wall. Widespread EGFP expression was confirmed before tissue harvest. The tissue appears normal despite cre-mediated recombination, which may include LSL-$Kras^{G12D}$. Five separate images were acquired and stitched via software. The stitching process required conversion to greyscale; no other alterations were made.

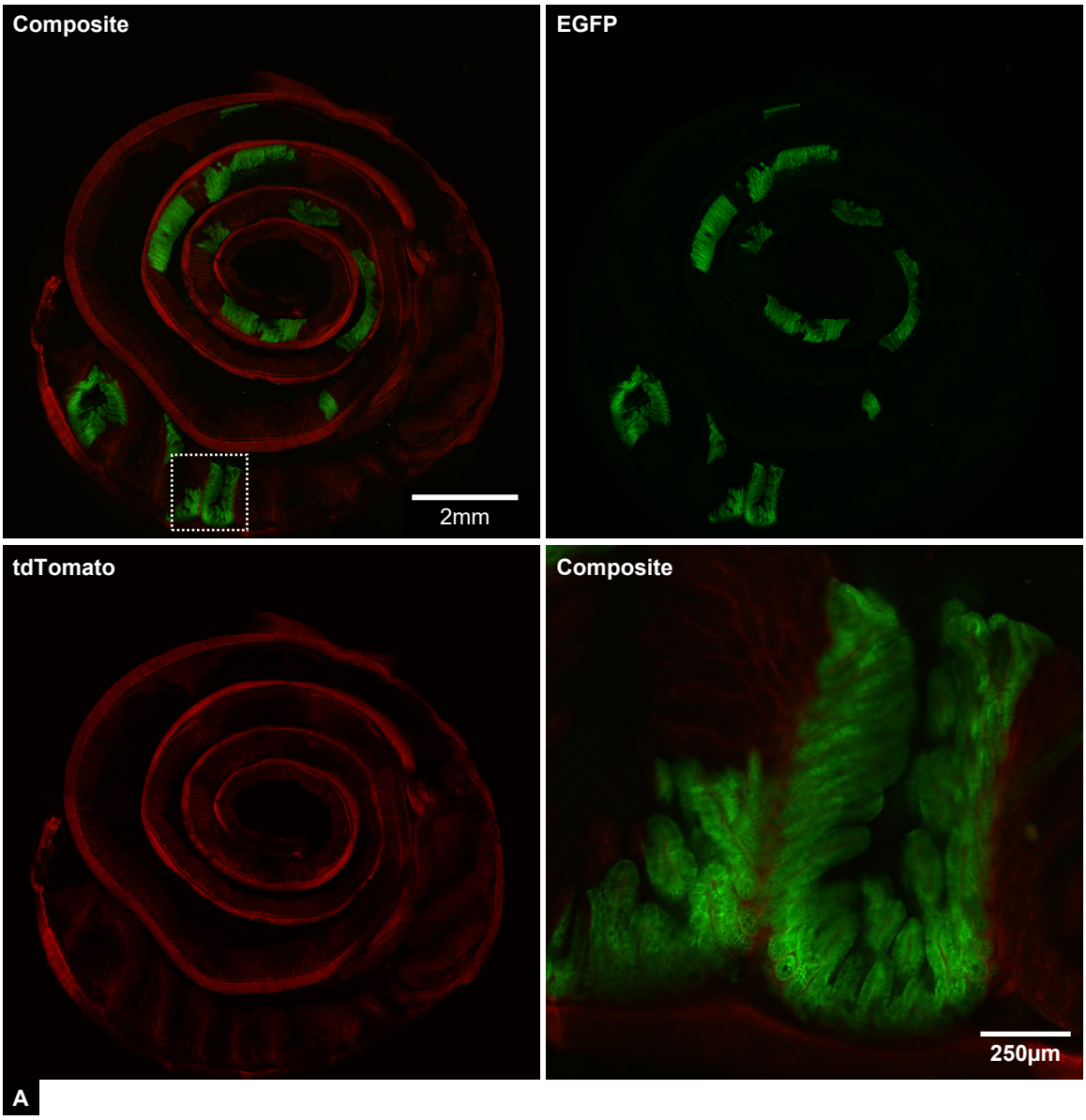
Composite
2mm
EGFP
tdTomato
Composite
250µm
A

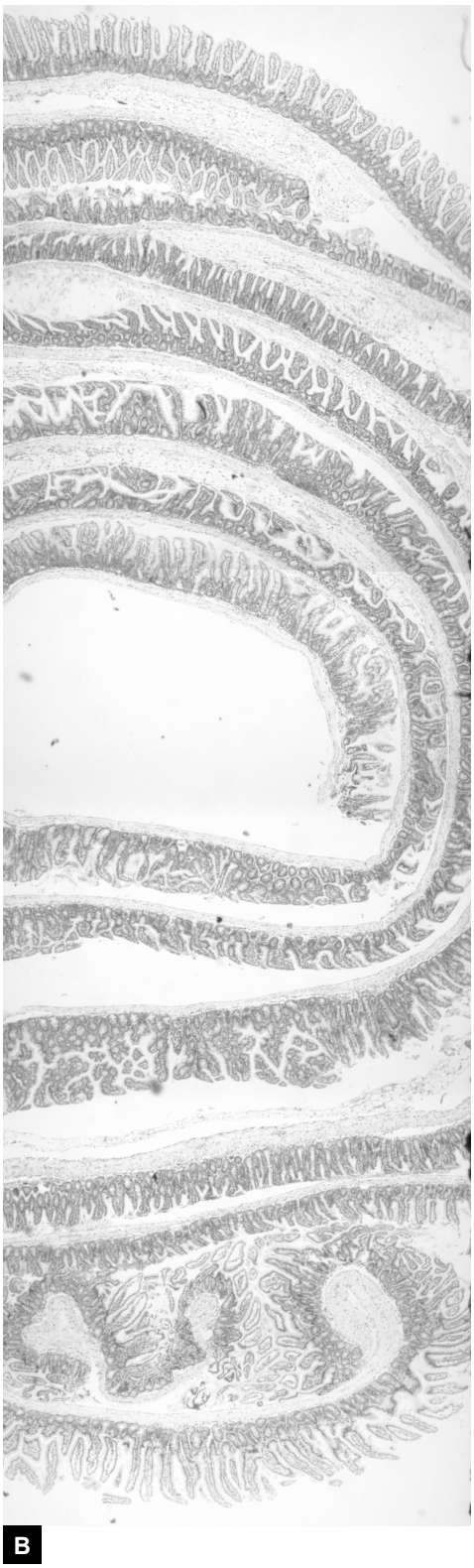

Figure 11. Histology and fluorescence microscopy of the CKmTmG large intestine microenvironment, continued

Acknowledgements

This chapter includes material currently published by: Cynthia S. Snyder, MD, Austin R. Harrington, BS, Sharmeela Kaushal, PhD, Evangeline Mose, BS, Andrew M. Lowy, MD, Robert M. Hoffman, PhD, and Michael Bouvet, MD, A Dual-Color Genetically Engineered Mouse Model for Multispectral Imaging of the Pancreatic Microenvironment. 2013; Pancreas.

DISCUSSION

Development and characterization of the PDX1-Cre/mTmG mouse model

Our studies showed the PDX1-Cre/mTmG mouse model produced intense membrane-bound EGFP expression in pancreatic epithelium (acinar cells, ducts, and islets), the proximal duodenum, and the caudal surface of the antral stomach; in contrast, all other tissue and cell types, including pancreatic stroma, expressed bright membrane-bound tdTomato fluorescence. Meanwhile, control mice lacking the PDX1-Cre construct expressed tdTomato in all tissues. Previous studies have shown pancreatic expression of fluorescent proteins may be particularly robust relative to that of other organs.[16] While this characteristic was observed in the PDX1-Cre/mTmG mouse and PDX1-Cre-negative controls, the precise mechanism for this effect is unknown but may be due to synergistic effects among the (very bright) EGFP and tdTomato fluorophores,[17] the cell density and corresponding membrane quantity of the murine pancreas, the structure of the exocrine pancreas microvasculature acting to limit the presence of spectrally-absorbent hemoglobin[18,19] or elevated activity of the CMV b-actin enhancer-promoter[14] driving mT/mG fluorescent protein expression in pancreatic tissue.

Though PDX1-Cre mediated recombination of the mTmG transgene was highly successful in most pancreata, we did observe mosaicism in our mice in the form of tdTomato-expressing pancreatic epithelium. Pancreatic mosaicism has been observed in previous studies examining both endogenous PDX1 activity and PDX1-Cre expression in developing and post-natal mice, though these studies used more primitive reporter constructs and immunostaining to visualize results.[20-23] The precise mechanisms for this mosaicism are manifold and not fully characterized. Contributing factors may include spatiotemporal separations of peak PDX1 activity among the progenitors of acini, ducts, and islets and among developing acini, ducts, and epithelial cell cords during development;[24, 25] mouse strain background may also have an effect. These studies

(including our own) did not specifically address endogenous mosaicism; however, PDX1-knockout mice develop severely stunted pancreata (an ultimately lethal phenotype), suggesting a basis other than a lack of PDX1 activity for pancreatic mosaicism.[21] Further evidence against that explanation comes from our study in the form of highly mosaic pancreata which were fully developed and functional (Figure 3E). In our PDX1-Cre/mTmG mouse line, a likely explanation for PDX1-driven pancreatic mosaicism was a threshold effect stemming from overall level of PDX1 activity and inherent probability of successful Cre recombination once expressed. Additionally, the brief period in which PDX1 is highly active in developing duct and acinar cells limits the time in which any PDX1-driven system (including Cre recombinase) may be active and successfully execute its desired activity. In developing duct and acinar cells which did not undergo successful rearrangement of the mTmG transgene, brief and low level PDX1 activity (and thus low PDX1-Cre expression) were the likely culprits.

Initial confocal imaging studies yielded more detailed observations of pancreatic mosaicism. Notably, mosaicism in pancreatic epithelium occurred only in discrete clusters rather than within individual cells; concurrent expression of both tdTomato and EGFP within a single cell produces a yellow signal in spectral composites,[14] a phenomenon we did not observe. The binary nature of fluorescence in cells indicates PDX1-Cre recombination of mTmG in acinar and duct cells must occur early in pancreatic development; membrane-bound tdTomato present prior to PDX1 activation is eventually degraded or removed from cell membranes and replaced by membrane-bound EGFP. Acinar and duct cells which fail to undergo the tdTomato to EGFP expression switch during development have little if any chance to recombine mTmG at a later point due to minimal PDX1 activity after gestation;[26] this suggests a clonal relationship among adjacent tdTomato-expressing acinar cells and/or duct cells that compose mosaic clusters.

Unlike acinar and ductal epithelium, pancreatic islet β cells (which compose

roughly 85% of mouse islets)[27] maintain a high level of PDX1 activity in perpetuity;[28, 29] consequently, we observed no mosaicism in islets. Despite their sustained PDX1 expression, confocal imaging of islets in cryosectioned pancreata from our PDX1-Cre/mTmG line showed them to produce weaker EGFP fluorescence than adjacent exocrine epithelium; stromal elements of both endocrine and exocrine tissue generated comparable tdTomato fluorescence. Potential mechanisms for this finding in islets include lower mTmG expression from the ROSA26 insertion locus relative to acinar and duct cells, inherent structural or functional differences between pancreatic exocrine and endocrine cell membranes, or the result of fluorescence quenching by hemoglobin due to the highly vascularized architecture of pancreatic islets, which receive approximately ten times more blood flow than exocrine pancreas by tissue volume.[18, 19]

Subsequent confocal imaging studies with fixed whole-mount tissue revealed the pancreatic microenvironment in stunning detail. Fixation appeared to have no adverse effects on the suitability and brightness of membrane-bound tdTomato and EGFP proteins for confocal imaging; photobleaching was not observed even during extended imaging sessions. Tissue remained suitable for further imaging even after several weeks when stored in phosphate buffered saline at 4°C. Using optical sectioning and standard deviation projections, we visualized the pancreatic microenvironment in three dimensions with great clarity to a depth of 30μm. Pancreatic microvasculature in particular benefits from these imaging techniques; acinar and ductal epithelium was expectedly dense and highly fluorescent, with only the occasional acinar cluster lumen clearly discernable. Other investigators have examined the pancreatic microenvironment in similar detail but relied on complex systems of vascular perfusion, immunostaining, single-fluorescent mice, and optical clearing techniques.[30] Our dual-fluorescent system is nearly as effective for imaging and confers other benefits such as the potential for lineage tracing while requiring much less tissue processing; however, combining elements

of both labelling techniques could provide new insights into the pancreatic microenvironment that neither system could achieve alone.

Mosaic EGFP expression was also observed in the small intestine of the PDX1-Cre/mTmG mouse line. EGFP fluorescence was strongest in the most proximal region of the duodenum (especially near the pylorus) and expression decreased distally down the length of the duodenum becoming more dappled until fading away entirely; occasional detections of EGFP in the jejunum, ilium, cecum, and colon were minimal and confined to very small clusters of epithelial cells (Figure 6C). The presence of EGFP expression in the duodenum was not unexpected given its developmental relationship to the pancreas; several studies using PDX1 reporter constructs have described PDX1 activity similar to our own observations.[20-22,31]

We further scrutinized gastrointestinal EGFP mosaicism via multiphoton and traditional confocal microscopy. Multiphoton imaging of the duodenum (distal of the pylorus) permitted detailed visualization of the duodenal microenvironment with nearly 200μm of imaging depth. This imaging enabled examination of the various tissue layers of the duodenum including the muscularis and outermost vasculature, type IV collagen connective tissue, and epithelium of the mucosa. Most cells, including much of the mucosal epithelium, expressed tdTomato; however, discrete clusters of EGFP-expressing epithelium (mosaicism) were also observed. Type IV collagen was detected due to its ability to generate a second harmonic signal.[32] The resolution and depth penetration afforded by multiphoton confocal imaging and fluorescent characteristics of our tissue samples enabled easy three-dimensional reconstruction of a small region of the duodenal microenvironment (Figure 6A); such a technique could be useful to further study the duodenal microenvironment in the context of lineage tracing studies and to further investigate the characteristics of PDX1 mosaicism in duodenal development of submucosal glands and villi.[33,34]

To examine the most of extreme cases of EGFP mosaicism in the gastrointestinal tract we adapted the classic “Swiss Roll” technique[34] for confocal imaging and examined a long section of the PDX1-Cre/mTmG mouse colon wall. This revealed small, discrete clusters of EGFP-expressing epithelium in the mucosa of the large intestine; interestingly, the morphology of EGFP-expressing cells appeared identical to that of neighboring tdTomato-expressing epithelium. In line with previous studies examining the role of PDX1 in gut development, this finding indicates PDX1 was not deterministic in the process of the final identity and clonal expansion of the observed EGFP-expressing cells into normal colon epithelium.[36] Mechanisms for how this population of cells with PDX1 activity transited to the colon are mostly speculative; some cells from the duodenum may drift across the gap between the two extreme ends of the developing gut (a mechanism contributing to the expansion and migration of the developing gastrointestinal neural crest)[37], or a small population of cells with PDX1 activity most distal to the duodenum are sequestered to the distal bowel by expansion of the jejunum and ilium between the colon and the duodenum. In either mechanism, this population cells with PDX1 activity must clonally expand to form discrete regions of EGFP-expressing epithelium as no single EGFP-positive cells were detected.

Overall, the PDX1-Cre/mTmG mouse model demonstrates several characteristics which could be of immense value in a wide variety of experimental settings. Of extreme usefulness is the ability to co-excite and co-detect tdTomato and EGFP using a single excitation and emission filter set, while retaining the ability to capture each channel individually. This is made possible by both the extreme brightness of tdTomato and its excitation curve which, overlaps that of EGFP; however, the emission peaks of tdTomato and EGFP are sufficiently spectrally separated to filter one signal from the other if desired.[17, 38] Additionally, the gene encoding tdTomato and EGFP is heritable during clonal expansion, membrane-targeted EGFP and tdTomato proteins are highly

stable, extremely bright, non-toxic, and do not diffuse across membranes to adjacent cells; as such, this mouse line provides extremely sharp membrane resolution and easy differentiation between cells of different lineages. Lineage tracing via fluorescence is already a well-established method used in the fields of developmental and cancer biology;[29, 39-41] use of multiple fluorescence constructs is an emerging technique and enables investigators to purse more varied and specific lines of inquiry.[43, 44] The PDX1-Cre/mTmG line could be well-utilized in studies examining lineage tracing and tissue architecture to enhance current knowledge of pancreatic (and perhaps duodenal) disease.

Development and characterization of the CKPmTmG mouse model

After developing and characterizing the dual-fluorescent PDX1-Cre/mTmG mouse model, we chose to investigate its potential applications. To that end we intercrossed the PDX1-Cre/mTmG mouse line with mice bearing the conditional LSL-Kras$^{G12D/+}$ and LSL-Trp53$^{R172H/+}$ knock-in transgenes first combined in the well-characterized mouse model of pancreatic cancer developed by Hingorani and colleagues. Upon successful breeding of we generated quadruple-transgenic mice bearing PDX1-Cre (C), mTmG, LSL-Kras$^{G12D/+}$ (K), and LSL-Trp53$^{R172H/+}$ (P), which we refer to as “CKPmTmG;” like their triple-transgenic predecessors, these mice developed pancreatic tumors leading to significant morbidity early in life leading to premature death from disease.[8]

However, unlike the CPK mouse line, our CKPmTmG developed tumors in which stromal components expressed tdTomato and epithelial-derived tissue expressed EGFP. These tumors developed a wide range of pathologic features; many of these were observable at the macroscopic level of imaging due to highlighting of structures by dual-fluorescent color coding. Gross anatomical findings included abdominal ascites, serous cystic pancreatic masses, acinar tissue atrophy, and solid pancreatic tumors. Many of the solid tumors were covered in highly-dilated and distended duct-like

structures expressing EGFP; examining these abnormal ducts in tdTomato channels revealed their underlying architectural support.

Macroscopic imaging showed marked differences in relative pancreatic fluorescence intensity between CKPmTmG mice with pancreatic tumors and unaffected controls. Overall, tdTomato fluorescence in the pancreata of CKPmTmG mice significantly increased relative to that observed in control mice; this finding is consistent with the distinct proliferation of pancreatic stroma (which expresses tdTomato in our model) characteristic of pancreatic cancer development.[44] Meanwhile, EGFP expression within pancreatic tumors was markedly decreased relative to that in the pancreata of controls; numerous mechanisms are believed to contribute to dropout of epithelial-derived tissue during development of PDAC, several of which are consistent with the pathologic findings we observed in the CKPmTmG mouse line. During the PanIN stages of PDAC development, obstruction of ducts may lead to the formation of cysts which contribute to acinar atrophy; this may also be accompanied by aberrant zymogen activation (particularly trypsinogen to trypsin) in the lumen of acini leading to further tissue breakdown.[45] Later in PDAC development, proliferation of pancreatic stromal tissue (desmoplasia) generates a hypoxic environment around epithelial-derived cells, precipitating significant cell dropout.[46] Cyst development and desmoplasia were common findings in CKPmTmG mice and CKmTmG mice.

Histological examination of CKPmTmG tumors showed features from the full range of PDAC development and provided structural explanations for findings made via fluorescence imaging. We documented ductal atypia, ductal dysplasia, duct-centered desmoplasia, acinar tissue atrophy and progressive isolation of islets, and high-grade malignancies exhibiting a high mitotic rate and associated nuclear abnormalities. Observations also included the full range of PanIN stages: the flat, columnar epithelium characteristic of PanIN-1A; papillary epithelium of PanIN-1B; papillary morphology, loss

of polarity, and nuclear crowding of cells typical of panIN-2; and distinctive architectural atypia, cribiforming, budding off of cell clusters, and luminal necrosis of PanIN-3.[47, 48]

Confocal imaging of CKmTmG pancreata exhibited the extreme power of the $Kras^{G12D}$ mutation to initiate the PanIN stages of PDAC development.[49] Our findings agree with previous documentation of $Kras^{G12D}$ acting through multiple autocrine and paracrine pathways to encourage fibroblast proliferation, angiogenesis, and other features which result in a pro-tumorigenic microenvironment.[50, 51] Depth projection of high resolution and high magnification sections of the tissue enabled detailed topographical examination of the cellular features in CKmTmG mice; the primary finding was of tissue in the PanIN-1A and PanIN-1B stages of PDAC development bearing large cystic regions, significant desmoplasia, and early isolation of islets. Acinar tissue was noticeably reduced in affected pancreata relative to those of PX1-Cre/mTmG, indicating a significant portion of the reduction in EGFP signal observed in CKPmTmG (and CKmTmG) occurs due to mechanisms early in the evolution to full PDAC. Interestingly, islets presented with none of the reduced EGFP fluorescence signal we observed in of frozen sections of the PDX1-Cre/mTmG pancreas; this effect could be due to a reduction in vascular hemoglobin via washout due to tissue immersion in fixative and phosphate buffered saline, reduced spectral absorption capability of hemoglobin post-fixation, enhanced membrane integrity imparted by fixation, or a combination of the above.

Mosaicism in the CKmTmG pancreas was more difficult to detect than that of PDX1-Cre/mTmG mice, but present in several forms. Some lobules of acinar and duct tissue presented with completely normal morphology and expressed tdTomato, indicating complete failure of PDX1-Cre to recombine mTmG in their common progenitor; others similarly presented with tdTomato-expressing acinar tissue (as aforementioned) but with lumens draining into EGFP-expressing ducts with normal morphology, indicating PDX1-Cre recombination success of the mT/mG transgene but failure to recombine

LSL-Kras$^{G12D/+}$. A third form of mosaicism was observed in a lobule of EGFP-expressing tissue with normal morphology of both acinar and duct components, indicating success of mTmG recombination but failure of LSL-Kras$^{G12D/+}$ recombination. Several of these findings have been documented in studies of PDX1 activity in the murine pancreas;[20] however, the mTmG transgene makes these features far easier to document.

One of the most unexpected features of the CKPmTmG mouse line were extreme levels of extrapancreatic EGFP expressed throughout the intestinal epithelium of these mice, especially in their colons. Though we had previously documented PDX1 activity in small, isolated clusters in the colons of PDX1-Cre/mTmG mice, the addition of the Kras^{G12D} or Trp53^{R172H} constructs to the line significantly elevated this effect. Statistical analysis of the distributions of EGFP expression in CKPmTmG, CPmTmG, CKmTmG, and PDX1-Cre/mTmG intestines indicated the expanded regions of PDX1 activity were tied specifically to inheritance of the LSL-Kras$^{G12D/+}$ construct. Previous studies using the CKP mouse model (or its variants) of pancreatic cancer, were not designed with a reporter construct that could have detected this characteristic of the CKP gastrointestinal tract.[8, 9] Examination of large bowel walls of CKPmTmG mice and its sub-genotypes via histology and confocal imaging indicated no abnormal tissue growth, such as that associated with colorectal cancer. This null finding concurs with current research indicating oncogenic Kras and loss of p53 are not imitators of colorectal cancer.[52-54] Ras is known to enhance migratory capability of cells which harbor oncogenic ras mutations, including those in Kras.[55, 56] Mechanistically, the observed expansion of EGFP-expressing epithelium in the large intestines of our CKPmTmG mice is likely similar to the proposed mechanisms previous discussed; however, the presence of an activated LSL-Kras$^{G12D/+}$ construct appears to enhance the process or confer greater potential for expansion once cells with a history of PDX1 activity colonize the distal bow-

el.[57, 58]

The CKPmTmG model demonstrates the full range of pathologic characteristics typical of the well-established CKP model of murine pancreatic cancer but affords great investigative advantages by endogenously labeling tissues of different lineages with the binary fluorescence expression system of mTmG. Investigations into heretofore unanswered aspects of the kinetics of developing PDAC, especially the process of the epithelial to mesenchymal transition (EMT), could be aided by fluorescence labelling.[51, 56] Some groups have already examined parts of this process but lacked an optimized system for addressing the precise processes involved in the EMT that occurs in pancreatic cancer; existing results are intriguing enough to warrant follow up and confirmation.[9] Dual-fluorescence labeling by mTmG also confers benefits to the processes of primary cell culture and sorting of cells derived from the CKPmTmG pancreas.[59, 60] Additional possibilities for its future use include lineage tracing of fluorescent xenograft transplants or use in mice with inducible PDX1-Cre constructs such as PDX1-CreER,[61] which may be useful for examining the development and progression of PDAC from a single locus. One area already explored by our characterization of this model is enhanced tissue imaging and three-dimensional analysis; further refinements could be made by exploiting emerging techniques in tissue imaging such as multiphoton confocal microscopy, membrane clearing, and addition of dyes and fluorescent antibodies to expand the range of features which may be studied and research questions which could be addressed.[30, 62] Even traditional investigative techniques like cryosectioning and immunohistochemistry could benefit from the tissue-specificity of mTmG dual-fluorescent protein expression by providing membrane labelling and high-contrast spectra in addition to selected antibody fluorescence. In the emerging field of immunotherapy for PDAC, the CKPmTmG mouse model could be an ideal organism for study by providing investigators with easily measurable stromal and epithelial derived tissue regions for quantification of therapy

efficacy.[63, 64] In conclusion, the CKPmTmG line of spontaneously generating murine pancreatic cancer could have a wide range of applications in the study of pancreatic ductal adenocarcinoma.

Acknowledgements

This chapter includes material currently published by: Cynthia S. Snyder, MD, Austin R. Harrington, BS, Sharmeela Kaushal, PhD, Evangeline Mose, BS, Andrew M. Lowy, MD, Robert M. Hoffman, PhD, and Michael Bouvet, MD, A Dual-Color Genetically Engineered Mouse Model for Multispectral Imaging of the Pancreatic Microenvironment. 2013; Pancreas.

REFERENCES

1. Hoyert, D.L. and Xu, J. (2012). Deaths: Preliminary Data for 2011. National Vital Statistics Report vol. 61, 52 pgs

2. Siegel, R., and Jemal, A. (2013). Cancer Facts & Figures 2013 (Atlanta: American Cancer Society)

3. Haeno, H., Gonen, M., Davis, M.B., Herman, J.M., Iacobuzio-Donahue, C.A., Michor, F. (2012). Computational Modeling of Pancreatic Cancer Reveals Kinetics of Metastasis Suggesting Optimum Treatment Strategies. Cell vol. 148, 632-375

4. Tuveson, D.A., Neoptolemos, J.P. (2012). Understanding Metastasis in Pancreatic Cancer: A Call for New Clinical Approaches. Cell vol. 148, 21-23

5. Lowy A.M., Leach S.D., and Philip P.A., eds. (2008) Pancreatic Cancer: M. D. Anderson Solid Tumor Oncology Series (New York: Springer Science+Business Media, LLC)

6. Metildi, C.A., Kaushal, S., Hardamon, C.R., Snyder, C.S., Pu, M., Messer, K.S., Talamini, M.A., Hoffman, R.M., and Bouvet, M. (2012). Fluorescence-Guided Surgery Allows for More Complete Resection of Pancreatic Cancer, Resulting in Longer Disease-Free Survival Compared with Standard Surgery in Orthotopic Mouse Models. Journal of the American College of Surgeons vol. 215, 126-135

7. Metildi, C.A., Hoffman, R.M., and Bouvet, M. (2013). Fluorescence-Guided Surgery and Fluorescence Laparoscopy for Gastrointestinal Cancers in Clinically-Relevant Mouse Models. Gastroenterology Research and Practice vol. 2013, 8 pgs

8. Hingorani, S.R., Wang, L. Multani, A.S., Combs, C., Deramaudt, T.B., Hruban, R.H., Rustgi, A.K., Chang, S., and Tuveson, D.A. (2005). $Trp53^{R172H}$ and $Kras^{G12D}$ cooperate to promote chromosomal instability and widely metastatic pancreatic ductal adenocarcinoma in mice. Cancer Cell vol. 7, 469-483

9. Rhim, A.D., Mirek, E.T., Aiello, N.M., Maitra, A., Bailey, J.M., McAllister, F., Reichert, M., Beatty, G.L., Rustgi, A.K., Vonderheide, R.H., Leach, S.D., and Stanger, B.Z. (2012) EMT and dissemination precede pancreatic tumor formation. Cell vol 148, 349-61

10. Hoffman, R.M. (2008). Recent Advances on in vivo Imaging with Fluorescent Proteins. Methods in Cell Biology vol. 85, 485-495

11. Okabe, M., Ikawa, M., Kominami, K., Nakanishi T., and Nishimune Y. (1997), 'Green mice' as a source of ubiquitous green cells. FEBS Letters vol. 407, 313-319

12. Vintersten, K., Monetti, C., Gertsenstein, M., Zhang, P., Laszlo, L., Biechele, S., and Nagy, A. (2004). Mouse in red: Red fluorescent protein expression in mouse

ES cells, embryos, and adult animals. Genesis vol. 40: 241–246

13. Megason, S.G., Fraser, S.E. (2003). Digitizing life at the level of the cell: high-performance laser-scanning microscopy and image analysis for in toto imaging of development, Mechanisms of Development vol. 120, 1407-1420

14. Muzumdar, M.D., Tasic, B., Miyamichi, K., Li, L., Luo, L. (2007). A Global Double-Fluorescent Cre Reporter Mouse. Genesis vol. 45, 593-605

15. Snyder, C.S., Harrington, A.R., Kaushal, S., Mose, E., Lowy, A.M., Hoffman, R.M., and Bouvet, M. (2013). A Dual-Color Genetically Engineered Mouse Model for Multispectral Imaging of the Pancreatic Microenvironment. Pancreas vol. 42, 952-958

16. Cao, H.S.T., Kimura, H., Kaushal, S., Snyder, C.S., Reynoso, J., Hoffman, R.M., and Bouvet, M. (2009). The Cyan Fluorescent Protein (CFP) Transgenic Mouse as a Model for Imaging Pancreatic Exocrine Cells. JOP : Journal of the Pancreas vol 10, 152-156.

17. Shaner, N.C., Steinbach, P.A., and Tsien, R.Y. (2005). A guide to choosing fluorescent proteins. Nature Methods vol. 2, 905-909

18. Horecker, B.L. (1943) The absorption spectra of hemoglobin and its derivatives in the visible and near infra-red regions. J. Biol. Chem. vol 148, 173-183

19. Dolenšek, J., Rupnik, M. S., and Stožer, A. (2015). Structural similarities and differences between the human and the mouse pancreas. Islets vol. 7, e1024405

20. Gu, G., Dubauskaite, J., and Melton, D.A. (2002). Direct evidence for the pancreatic lineage: NGN3+ cells are islet progenitors and are distinct from duct progenitors. Development vol. 129, 2447-2457

21. Offield, M.F., Jetton, T.L., Labosky, P.A., Ray, M., Stein, R.W., Magnuson, M.A., Hogan, B.L.M., and Wright, C.V. (1996). PDX-1 is required for pancreatic outgrowth and differentiation of the rostral duodenum. Development vol. 122, 983-995

22. Gannon, M., Herrera, P.L., and Wright, C. V.E. (2000). Mosaic Cre-mediated recombination in pancreas using the pdx-1 enhancer/promoter. Genesis vol. 26, 143-144

23. Gannon M., Gamer L.W., and Wright C.V. (2001). Regulatory regions driving developmental and tissue-specific expression of the essential pancreatic gene pdx1. Dev Biol. vol. 238, 185-201

24. Guz, Y., Montminy, M.R., Stein, R., Gamer, L.W., Wright, C.V., and Teitelman, G. (1995). Expression of murine STF-1, a putative insulin gene transcription factor, in beta cells of pancreas, duodenal epithelium and pancreatic exocrine and endocrine progenitors during ontogeny. Development vol. 121, 11-18

25. Fujitani, Y., Fujitani, S., Boyer, D.F., Gannon, M., Kawaguchi, Y., Ray, M., Shiota, M., Stein, R.W., Magnuson, M.A., and Wright, C.V.E. (2006). Targeted deletion of a cis-regulatory region reveals differential gene dosage requirements for Pdx1 in foregut organ differentiation and pancreas formation. Genes & Development, vol. 20, 253-266

26. Wu, K.L., Gannon, M., Peshavaria, M., Offield, M.F., Henderson, E., Ray, M., Marks, A., Gamer, L.W., Wright, C.V., and Stein, R. (1997). Hepatocyte nuclear factor 3beta is involved in pancreatic beta-cell-specific transcription of the pdx-1 gene. Molecular and Cellular Biology, vol. 17, 6002–6013

27. Steiner, D. J., Kim, A., Miller, K., and Hara, M. (2010). Pancreatic islet plasticity: Interspecies comparison of islet architecture and composition. Islets vol. 2, 135-145

28. Ahlgren, U., Jonsson, J., Jonsson, L., Simu, K., and Edlund, H. (1998). β-Cell-specific inactivation of the mouse Ipf1/Pdx1 gene results in loss of the β-cell phenotype and maturity onset diabetes. Genes & Development vol 12, 1763-1768.

29. Holland, A.M., Hale, M.A., Kagami, H., Hammer, R.E., and MacDonald, R.J. (2002). Experimental control of pancreatic development and maintenance. Proceedings of the National Academy of Sciences of the United States of America vol. 99, 12236-12241

30. Fu, Y.Y., Lu, C.H., Lin, C.-W., Juang, J.H., Enikolopov, G., Sibley, E., Chiang, A.S., and Tang, S.C. (2010). Three-dimensional optical method for integrated visualization of mouse islet microstructure and vascular network with subcellular-level resolution. Journal of Biomedical Optics vol. 15, 046018:1-9

31. Wescott, M. P., Rovira, M., Reichert, M., von Burstin, J., Means, A., Leach, S.D., and Rustgi, A.K. (2009). Pancreatic Ductal Morphogenesis and the Pdx1 Homeodomain Transcription Factor. Molecular Biology of the Cell vol. 20, 4838-4844

32. Cox, G., and Kable, E. (2006). Second-harmonic imaging of collagen. Methods in Molecular Biology: Cell Imaging Techniques vol. 319, 15-35

33. Gao, N., LeLay, J., Vatamaniuk, M. Z., Rieck, S., Friedman, J.R., and Kaestner, K.H. (2008). Dynamic regulation of Pdx1 enhancers by Foxa1 and Foxa2 is essential for pancreas development. Genes & Development vol. 22, 3435-3448

34. Chen, C., Fang, R., Davis, C., Maravelias, C., and Sibley, E. (2009). Pdx1 inactivation restricted to the intestinal epithelium in mice alters duodenal gene expression in enterocytes and enteroendocrine cells. American Journal of Physiology - Gastrointestinal and Liver Physiology vol. 297, G1126–G1137

35. Moolenbeek, C., and Ruitenburg, E.J. (1981). The 'Swiss roll': a simple technique for histological studies of the rodent intestine. Laboratory Animals vol. 15, 57-59

36. Jonsson, J., Carlsson, L., Edlund, T., and Edlund, H. (1994). Insulin-promoter-factor 1 is required for pancreas development in mice. Nature vol. 371, 606-609

37. Lake, J.I., and Heuckeroth, R.O. (2013). Enteric nervous system development: migration, differentiation, and disease. American Journal of Physiology - Gastrointestinal and Liver Physiology vol. 305, G1–G24

38. Shaner, N.C., Campbell, R.E., Stainbach, P.A., Giepmans, B.N.G., Palmer, A.E., and Tsien, R.Y. (2004). Improved monomeric red, orange and yellow fluorescent proteins derived from Discosoma sp. red fluorescent protein. Nature Biotechnology vol. 22, 1567-1572

39. Buckingham, M.E. and Meilhac, S.M. (2011). Tracing cells for tracking cell lineage and clonal behavior. Dev Cell vol. 21, 394-409

40. Kretzschmar, K. and Watt, F.M. (2012) Lineage tracing. Cell vol. 148, 33-45

41. Talchai, C., Xuan, S., Lin, H.V., Sussel, L., and Accili, D. (2012). Pancreatic β-Cell Dedifferentiation As Mechanism Of Diabetic β-Cell Failure. Cell, vol. 150, 1223-1234

42. Liu, C., Sage, J.C., Miller, M. R., Verhaak, R.G.W., Hippenmeyer, S., Vogel, H., Foreman, O., Bronson, R.T., Nishiyama, A., Luo, L., and Zong, H. (2011). Mosaic Analysis with Double Markers (MADM) Reveals Tumor Cell-of-Origin in Glioma. Cell vol. 146, 209-221

43. Livet, J., Weissman, T.A., Kang, H., Draft, R.W., Lu, J., Bennis, R.A., Sanes, J.R., and Lichtman, J.W. (2007). Transgenic strategies for combinatorial expression of fluorescent proteins in the nervous system. Nature vol. 450, 56-62

44. Kong, X., Li, L., Li, Z., and Xie, K. (2012). Targeted Disruption of Orchestration between Stroma and Tumor Cells in Pancreatic Cancer: Molecular Basis and Therapeutic Implications. Cytokine & Growth Factor Reviews vol. 23, 343–356

45. Brune, K., Abe, T., Canto, M., O'Malley, L., Klein, A. P., Maitra, A., Adsay, N.V., Fishman, E.K., Cameron, J.L., Yeo, C.J., Kern, S.E., Goggins, M., and Hruban, R.H. (2006). Multifocal Neoplastic Precursor Lesions Associated With Lobular Atrophy of the Pancreas in Patients Having a Strong Family History of Pancreatic Cancer. The American Journal of Surgical Pathology vol. 30, 1067-1076

46. Xie, D. and Xie, K. (2015). Pancreatic cancer stromal biology and therapy. Genes & Diseases vol 2, 133-143

47. Hruban, R.H., Adsay, N.V., Albores-Saavedra, J., Compton, C., Garrett, E.S., Goodman, S.N., Kern, S.E., Klimstra, D.S., Klöppel, G., Longnecker, D.S., Lüttges, J., and Offerhaus, G.J. (2001) American Journal of Surgical Pathology vol. 25, 579-586

48. Hruban, R.H., Takaori, K., Klimstra, D.S., Adsay, N.V., Albores-Saavedra, J., Biankin, A.V., Biankin, S.A., Compton, C., Fukushima, N., Furukawa, T., Goggins, M., Kato, Y., Klöppel, G., Longnecker, D.S., Lüttges, J., Maitra, A., Offerhaus, G.J., Shimizu, M., and Yonezawa, S. (2004). An illustrated consensus on the classification of pancreatic intraepithelial neoplasia and intraductal papillary mucinous neoplasms. American Journal of Surgical Pathology vol. 28, 977-987

49. Smit, V.T., Boot, A. J., Smits, A.M., Fleuren, G.J., Cornelisse, C.J., and Bos, J.L. (1988). KRAS codon 12 mutations occur very frequently in pancreatic adenocarcinomas. Nucleic Acids Research vol. 16, 7773-7782

50. Pylayeva-Gupta, Y., Grabocka, E., and Bar-Sagi, D. (2011). RAS oncogenes: weaving a tumorigenic web. Nature Reviews Cancer, vol. 11, 761-774

51. Rachagani, S., Senapati, S., Chakraborty, S., Ponnusamy, M.P., Kumar, S., Smith, L.M., Jain, M., and Batra, S.K. (2011). Activated KrasG12D is associated with invasion and metastasis of pancreatic cancer cells through inhibition of E-cadherin. British Journal of Cancer, vol. 104, 1038-1048

52. Fearon, E.R. (2011). Molecular Genetics of Colorectal Cancer. Annual Review of Pathology: Mechanisms of Disease vol. 6, 479-507

53. Karim, B.O., and Huso, D.L. (2013). Mouse models for colorectal cancer. American Journal of Cancer Research vol. 3, 240-250

54. Markowitz, S.D., and Bertagnolli, M.M. (2009). Molecular Origins of Cancer: Molecular Basis of Colorectal Cancer. The New England Journal of Medicine vol. 361, 2449-2460

55. Stolze, B., Reinhart, S., Bulllinger, L., Fröhling, S., and Scholl, C. (2015). Comparative analysis of KRAS codon 12, 13, 18, 61, and 117 mutations using human MCF10A isogenic cell lines. Scientific Reports vol. 5, 8535

56. Bendris, N., Cheung, C.T., Leong, H.S., Lewis, J.D., Chambers, A.F., Blanchard, J.M., and Lemmers, B. (2014). Cyclin a2, a novel regulator of EMT. Cellular and Molecular Life Sciences vol. 71, 4881-4894

57. Bryant, K.L., Mancias, J.D., Kimmelman, A.C., and Der, C.J. (2014). KRAS: feeding pancreatic cancer proliferation. Trends in Biochemical Sciences vol. 39, 91-100

58. Hanahan, D. and Weinberg, R.A. (2011). Hallmarks of Cancer: The Next Generation. Cell vol. 144, 646-674

59. Li, D., Yuan, Y., Tu, H., Liang, Q., and Dai, L. (2009). A protocol for islet isolation from mouse pancreas. Nature Protocols, vol. 4, 1649-1652

60. Reichert, M., Takano, S., Heeg, S., Bakir, B., Botta, G.P., and Rustgi, A.K. (2013).

Isolation, culture and genetic manipulation of mouse pancreatic ductal cells. Nature Protocols, vol. 8, 1354-1365

61. Habbe, N., Shi, G., Meguid, R.A., Fendrich, V., Esni, F., Chen, H., Feldmann, G., Stoffers, R.A., Konieczny, S.F., and Maitra, A. (2008). Spontaneous induction of murine pancreatic intraepithelial neoplasia (mPanIN) by acinar cell targeting of oncogenic Kras in adult mice. Proceedings of the National Academy of Sciences of the United States of America vol.105, 18913-18918

62. Lin, P.Y., Peng, S.J., Shen, C.N., Pasricha, P.J., and Tang, S.C. (2016). PanIN-associated pericyte, glial, and islet remodeling in mice revealed by 3D pancreatic duct lesion histology. American Journal of Physiology - Gastrointestinal and Liver Physiology vol 311, G412-G422

63. Feng, M., Xiong, G., Cao, Z., Yang, G., Zheng, S., Song, X., You, L., Zheng, L., Zhang, T., and Zhao, Y. (2017). PD-1/PD-L1 and immunotherapy for pancreatic cancer. Cancer Letters vol. 407, 57-65

64. Foley, K., Kim, V., Jaffee, E., and Zheng, L. (2016). Current progress in immunotherapy for pancreatic cancer. Cancer Letters vol. 381, 244-251